Available online at www.sciencedirect.com
SCIENCE DIRECT®
Sedimentary Geology xx (2005) xxx–xxx
Sedimentary Geology
www.elsevier.com/locate/sedgeo

Carbonate deposition and hydrocarbon reservoir development at the Precambrian–Cambrian boundary: The Ara Group in South Oman

Stefan Schröder [a,b,*], John P. Grotzinger [b], Joachim E. Amthor [c], Albert Matter [a]

[a] *University of Bern, Institute of Geological Sciences, Baltzerstrasse 1, CH-3012 Bern, Switzerland*
[b] *Massachusetts Institute of Technology, Department of Earth, Atmospheric and Planetary Sciences, Cambridge, MA 02139, USA*
[c] *Petroleum Development Oman, P.O. Box 81, Muscat, PC 113, Sultanate of Oman*

Received 27 October 2004; received in revised form 13 June 2005; accepted 14 July 2005

Abstract

The Ediacaran–Early Cambrian Ara Group in the South Oman Salt Basin consists of six evaporite–carbonate cycles (A0/A1 to A6) that record tectono-eustatic sea-level changes. The A4 cycle developed at the Precambrian–Cambrian boundary (~542 Ma). It forms a single depositional sequence with evaporites deposited in a lowstand systems tract (LST). Overlying carbonates represent an open-marine shallowing-upward ramp succession that developed in transgressive (TST) and highstand systems tracts (HST). The low-energy carbonate ramp occupied a relatively protected site between a large shelf and an exposed paleogeographical high.

The TST facies include sulfates, evaporite–carbonate laminites, and organic-rich carbonate laminites that record initial flooding, deepening of the basin, and establishment of an outer ramp depositional environment. Carbonate sediment flux was low and the environment was partly subject to cyclically elevated salinity. Subsequent HST facies comprise mostly fine-grained clastic carbonates and stromatolites that formed in middle and inner ramp settings. These facies show evidence of shoaling and establishment of a carbonate factory that probably operated over most of the middle and inner ramp. Sediment was redistributed in suspension, by muddy turbidity currents, muddy debris flows, storm and shallow-water currents. During the late HST, carbonate facies were affected by elevated salinity and recorded the gradual transition to the overlying LST evaporite unit. A combination of strong tectonic subsidence and transient flooding caused significant shallow-water evaporite deposition to occur not only down dip, but also *on top* of the former carbonate platform, where several hundreds of meters of evaporites accumulated.

The transgressive carbonate laminites are the main reservoir facies and thus represent a relatively unusual reservoir unit. The presence of organic material and the relative scarcity of carbonate mud influenced diagenesis and reservoir properties. Distribution of organic material and carbonate mud can be linked to specific environmental conditions (low physical and biogenic disturbance of sediment and stratified water mass) and the sequence stratigraphic position (low flux of fine-grained

* Corresponding author. University of Johannesburg, Auckland Park 2006, Johannesburg, South Africa. Fax: +27 11 4892309.
E-mail address: sts@rau.ac.za (S. Schröder).

0037-0738/$ - see front matter
doi:10.1016/j.sedgeo.2005.07.002

carbonate during TST). In contrast, diagenetic evaporite formation has largely degraded reservoir quality in porous shallow-water facies near the top of the A4C.

Keywords: Ediacaran; Cambrian; Oman; Carbonate ramps; Sequence stratigraphy; Reservoir rocks

1. Introduction

Growing research has refined the picture of architecture, facies dynamics, biostratigraphy and chemostratigraphy of Precambrian carbonate platforms, placing them within the context of environmental and biological evolution (Grotzinger, 1989; Grotzinger and James, 2000, and references therein). Neoproterozoic and Ediacaran carbonates in particular are now well understood, with a level of detail that is similar to Phanerozoic platforms (e.g., Pelechaty et al., 1996; Turner et al., 1997; Adams et al., 2004; DiBenedetto and Grotzinger, in press; Grotzinger et al., in press). These rocks record significant environmental and biological changes and they include thrombolite buildups and the first skeletal metazoans that added to the complexity of carbonate facies and sediment production (Grotzinger and James, 2000; Hofmann and Mountjoy, 2001; Watters and Grotzinger, 2001; Wood et al., 2002; Grotzinger et al., in press). These elements, unknown from older Precambrian carbonates, represent precursors of younger carbonates that are strongly influenced by calcifying metazoans. However, to understand the impact of this evolutionary event on facies distributions in the Early Cambrian, it is critically important to establish a baseline of variability in carbonates of latest Neoproterozoic (Ediacaran) age.

The Ara Group in the subsurface of the South Oman Salt Basin (SOSB) provides such an oppor-

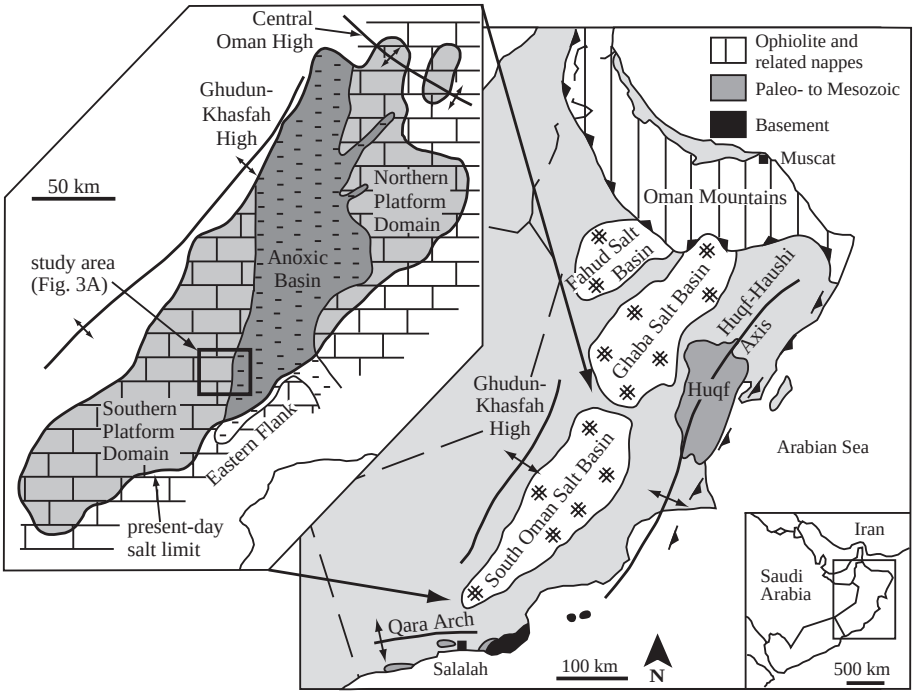

Fig. 1. Structural and paleogeographic setting of the study area. Large map shows overview of the interior Oman sedimentary basins with surrounding structural highs. Inset map illustrates paleogeography of the South Oman Salt Basin during the A4 cycle of the Ara Group. Study area is marked by black box (see Fig. 3A) (modified after Loosveld et al., 1996).

tunity (Fig. 1). The base of the carbonate platform studied here coincides with the Precambrian–Cambrian boundary in Oman (Fig. 2; Amthor et al., 2003). Recent studies of the Ara Group have demonstrated significant environmental changes leading to a negative carbon isotope excursion (Fig. 2) and the extinction of early calcified metazoans (Amthor et al., 2003). Thus, the Ara Group can provide insights into how these environmental changes influenced platform architecture, depositional processes and reservoir development across the Precambrian–Cambrian boundary. The studied

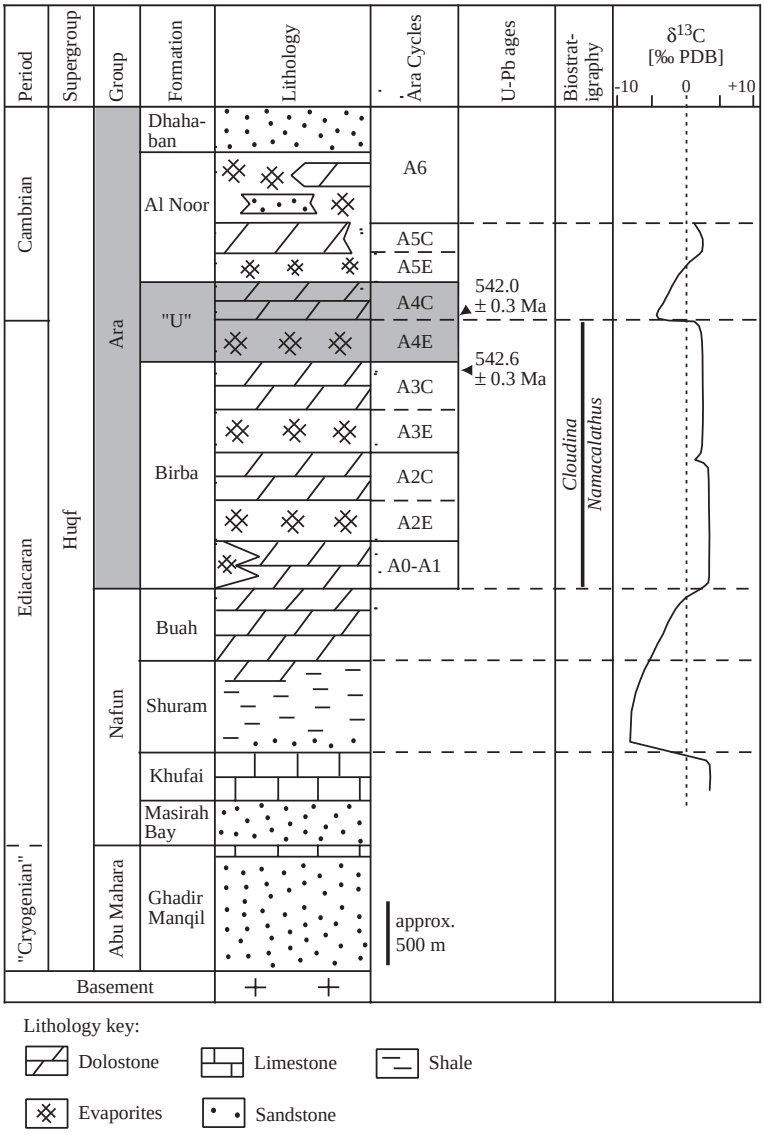

Fig. 2. Generalized stratigraphy of the Huqf Supergroup in the South Oman Salt Basin. The studied interval is highlighted in grey. Each Ara Group cycle contains an evaporitic unit (e.g., A4E) and a carbonate unit (e.g., A4C). Note that carbonate unit thicknesses have been exaggerated for readability. Zircons in volcanic tuffs of the Ara Group yielded ages of 542.0 ± 0.3 Ma, and 542.6 ± 0.3 Ma, respectively. Carbon isotopes and fossils support an Ediacaran–Cambrian age of the Ara Group (adapted from Burns and Matter, 1993; Loosveld et al., 1996; Amthor et al., 2003).

platform contains unusual oil reservoirs in deep-water, laminated, organic-rich carbonates sealed by evaporites (Mattes and Conway Morris, 1990; Grotzinger and Amthor, 2002). This study uses exploration drill cores to examine the spatial relationships between the different lithofacies and to derive a depositional, diagenetic and sequence stratigraphic model for the platform and the reservoir facies. The discussion emphasizes platform architecture, constraints on reservoir development, and implications for the sequence stratigraphy of the carbonate–evaporite transition.

2. Geological setting

The interior of Oman contains sedimentary basins that represent a major hydrocarbon province (Fig. 1; Loosveld et al., 1996). The basins developed on Neoproterozoic crystalline basement. Neoproterozoic to Early Cambrian strata of the Huqf Supergroup fill the lower parts of these basins (Fig. 2; Gorin et al., 1982; Mattes and Conway Morris, 1990; Loosveld et al., 1996). The age of the Ara Group, the main exploration target in the SOSB, is constrained by absolute U–Pb ages, carbon isotope stratigraphy, and paleontology (Fig. 2; Amthor et al., 2003).

The Ara Group contains six tectono-eustatic evaporite–carbonate cycles (A0/A1–A6); siliciclastic deposits occur at the top of the Ara Group (Fig. 2; Mattes and Conway Morris, 1990). The lower unit of each cycle is formed by evaporites that precipitated during basin restriction (e.g., unit A4E; Fig. 2). Evaporites are up to several hundred meters thick and commonly contain the characteristic succession anhydrite–halite–anhydrite (Schröder et al., 2003). Overlying carbonates are between 50 and 150 m thick (e.g., unit A4C; Fig. 2). They represent platform carbonates deposited under conditions of normal marine salinity (Mattes and Conway Morris, 1990). In sequence stratigraphic terms, Ara Group evaporite–carbonate cycles usually contain more than one depositional sequence. However, the A4 cycle of this study represents a single depositional sequence with evaporite deposition in the LST, and deposition of evaporites and carbonates in TST and HST.

The A4 cycle contains the Precambrian–Cambrian boundary, constrained by a volcanic tuff dated at 542.0 ± 0.3 Ma (Fig. 2; Amthor et al., 2003). During deposition of the A4 cycle, the SOSB was divided into three paleogeographic areas (Fig. 1). The northern and southern carbonate platform domains flanked an anoxic basin probably several hundred meters deep. Well data suggest that the southern platform domain represented a broad shelf with localized carbonate accumulations that formed isolated platforms of A1–A5 age. The Birba platform nucleated close to the eastern edge of this shelf, and contains a ≤ 80-m-thick A4 carbonate unit (A4C; Fig. 3A). Positive identification of the A4C relies on seismic data, lithostratigraphy, a distinctive gamma-ray spike that marks the dated tuff, and negative inorganic carbon isotopes (Fig. 3B; Amthor et al., 2003, 2005). These data suggest that the A4C thins below seismic resolution west of the Birba platform, where the A4 cycle is entirely evaporitic (Fig. 3B). Due to high subsidence east of the shelf edge, A4C-equivalent shales and cherts were deposited in the adjacent deep basin (Fig. 3B).

Wells through the eastern edge of the intra-platform shelf contain stacked carbonates without evaporites, and facies include thrombolite buildups, shallow-water facies and karst (Fig. 3B; Pope et al., 2000; Schröder, 2000). The gamma-ray spike and the carbon isotope anomaly are absent, and carbonates are overlain by evaporites of the A5 cycle (Fig. 3B). Consequently, these carbonates are older than the A4 cycle. The shelf edge may have been exposed during deposi-

Fig. 3. (A) Detailed paleogeography of the Birba carbonate platform during deposition of the A4 carbonate. The shaded area defines the known extent of the Birba platform, based on seismic and well data. It was probably attached to the shelf edge of the intra-platform shelf, but no data are available for the transition zone (hatching). The western margin of the central anoxic basin may have been constructional or structural. (B) Available well data for the Birba platform. The shaded section represents known A4 carbonate. Cherty shales are equivalent to the A4 carbonate in the deep basin. Carbon isotope data were available only for wells BB-4 and SB-1 and are given in ‰PDB (data from Amthor et al., 2003 and previously unpublished data). (C) Conceptual cross-section over the platform to illustrate overall platform geometry and the position of the major paleogeographic features. The shaded area defines known occurrence of the A4 carbonate.

tion of the A4C, or any deposited A4C was subsequently removed by erosion. Given the karstified carbonates, the first interpretation is preferred here, and the Birba ramp onlapped and was attached to the paleogeographical high at the shelf edge (Fig. 3C; Amthor et al., 2005).

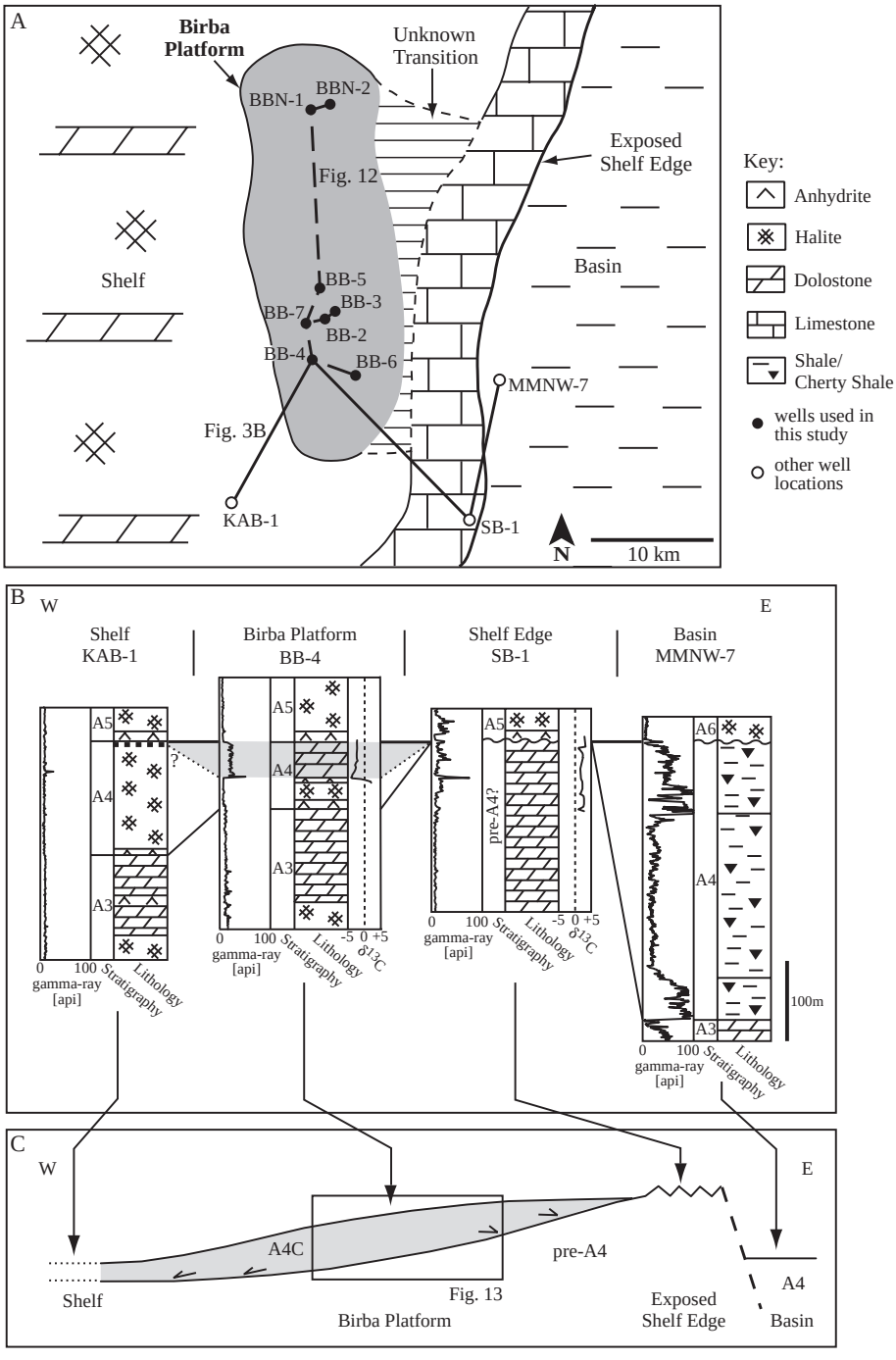

3. Facies analysis

3.1. Stratigraphic framework and vertical succession

The facies succession of the A4 cycle includes lowstand evaporites overlain by carbonate ramp deposits (Mattes and Conway Morris, 1990). Rapid deepening at the base was followed by shoaling to sea level (Fig. 4; Mattes and Conway Morris, 1990). The lithofacies are grouped into outer ramp, middle ramp and inner ramp facies, evaporite–carbonate transition and associated facies (Fig. 4 and Table 1). The follow-

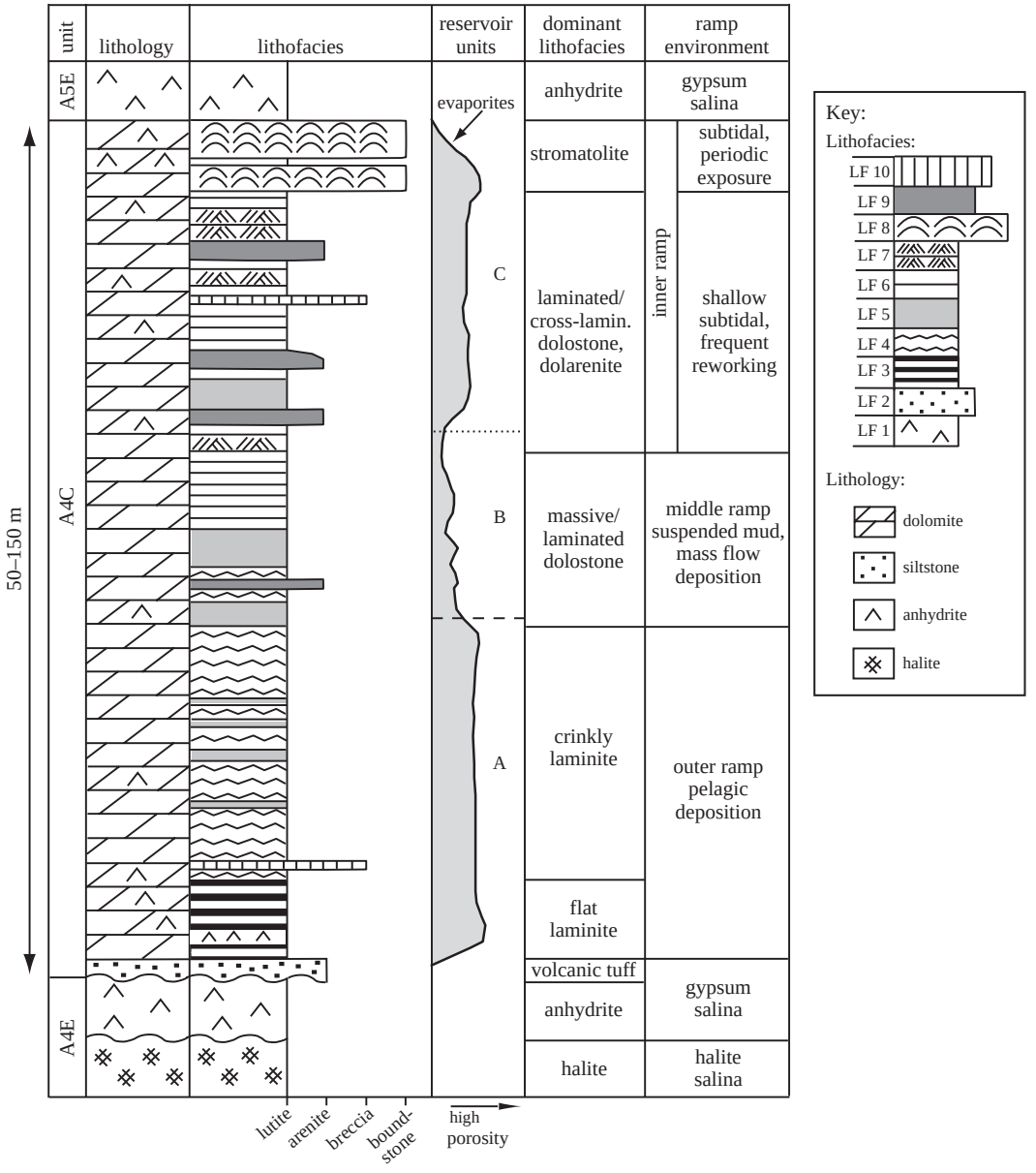

Fig. 4. Summary log of the A4 carbonate, showing the vertical succession of lithofacies on the left and the different ramp environments on the right. Porosity distribution is given as a proxy for reservoir quality in the three reservoir units A (good reservoir properties), B (poor reservoir properties), and C (intermediate–good reservoir properties). See text for discussion.

Table 1
Detailed description of A4 carbonate lithofacies

Lithofacies	Occurrence and thickness	Sedimentary structures	Components and microfacies	Remarks
Evaporite–carbonate transition				
LF 1 Anhydrite	A4 and A5 evaporite units; sharp contact A4E to A4C, gradual transition A4C to A5E via interbedded anhydrite	Nodular, bedded and massive anhydrite; upright palmate nodules after selenite gypsum; rare desiccation cracks	Micritic dolomite between nodules, laminar chevron dolomite inclusions	
LF 2 Volcanic tuff Fig. 6	Sharply overlying LF 1 at base of A4C; up to a few decimeters thick; top gradual to LF 3	Faint millimetric lamination to mottled and streaky; graded, load casts and desiccation cracks; skeletal halite casts with clastic sediment fill	Sand- and silt-sized quartz, feldspar, scattered pyrite, volcanic zircons (size 50–100 μm) and glauconite, (sub)angular grains; matrix with micritic dolomite, microcrystalline anhydrite and deformed displacive anhydrite nodules	
Outer ramp				
LF 3 Flat laminite Fig. 7A–B	Lowermost carbonate unit of A4C; thickness 2–3 m; top gradual to LF 4; near base centimeter-thick intercalations of LF 1 with sharp contacts	Millimetric even laminated dolo-lutite and anhydrite (varves) with slumps, drag folds, kink bands and small faults; transition between laminae gradual or sharp; rare erosive bases of anhydrite laminae	*(1) Alternation dolomite–anhydrite*. Fine crystalline, euhedral to anhedral dolomite; small laths or equant blocky anhydrite crystals (size 10 μm to 10×200 μm), laths often parallel to lamination; anhydrite contents $\leq 50\%$ *(2) All laminae dolomitic*. Finely crystalline anhedral crystals in dark laminae, medium crystalline euhedral crystals in light laminae; some laminae with peloids (diameter 50–110 μm) aligned parallel to lamination	No porosity; some laminae replaced by quartz and brecciated

(continued on next page)

Table 1 (*continued*)

Lithofacies	Occurrence and thickness	Sedimentary structures	Components and microfacies	Remarks
Outer ramp				
LF 4 Crinkly laminite Fig. 7C–D	Thickness ~15 m; top gradual to LF 5 via thickening of light laminae and increasing abundance of LF 5 interbeds; some millimeter- to centimeter-thick interbeds of LF 10 ± LF 9	Sub-millimetric to millimetric crinkly laminated dolomite; slumping, in-situ brecciation, small-scale thrusts	*Dark laminae* with finely crystalline dolomite, partly micritic; slightly clotted microfabric; laminae rarely discontinuous, including lenses of coarser dolomite; relatively organic-rich	Pinpoint (vuggy) porosity common near base of light laminae, intercrystalline porosity
		Dark laminae with flat base and millimeter-scale irregularities at top, relief draped by *light laminae*; chips of dark laminae incorporated in light laminae	*Light laminae* with medium to finely crystalline dolomite (coarser than in dark laminae), often normal graded crystal size, idiotopic texture	
Middle ramp				
LF 5 Massive dolostone Fig. 9A	Basal unit of middle ramp; top gradual to LF 6; bedsets several decimeter-thick and millimeter- to decimeter-thick interbeds in crinkly laminites, sharp contacts	Clean structureless dolostone, rare wispy lamination; rare erosion surfaces	Finely to medium crystalline dolomite, idiotopic to xenotopic texture; ?intraclasts suggested by different dolomite crystal size and porosity	Intercrystalline porosity and few rounded oversized vugs
LF 6 Laminated dolostone Fig. 9B	Thickness combined with LF 5 is ~9 m; centimeter to decimeter interbeds of LF 9 and LF 10 most common in well BB-3	Similar to LF 5, but millimeter- to centimeter-scale lamination, even to wavy, often wispy; rare erosion surfaces	Lamination determined by graded crystal size, and by solution seams/stylolites creating a secondary stylo-lamination	Intercrystalline porosity
Inner ramp				
LF 7 Cross-laminated dolostone Fig. 9C	Interstratified with massive (LF 5) and laminated (LF 6) beds; increase in abundance up-section	Millimetric ripple-lamination, planar cross-lamination, low-angle trough cross-lamination, and ?swaley cross-lamination; rare erosion surfaces	Microfacies similar to LF 5 and LF 6	Originally silt- to sand-sized clastic carbonates

LF 8 Stromatolite Fig. 10	Top 5–15 m of A4C; interbes of LF 1 in transition to A5E; LF 5 and LF 9 form centimeter-thick interbeds with well-defined and erosive contacts	Stratiform, LLH- and SH-type stromatolites, rare columnar-tufted stromatolites; millimeter- to centimeter-sized domes, transitional to wavy laminated mudstones (LF 6); additional dendritic and chevron structures, isopachous and fenestral stromatolites; recrystallized? thrombolites at top of BB-5; desiccation cracks, scouring surfaces	Stratiform, LLH, SH and columnar-tufted with discontinuous uneven lamination; micritic to strongly recrystallized dolomite, replacive evaporites and evaporite cements	Intercrystalline and vuggy porosity
Associated facies				
LF 9 Dolarenite Fig. 11A–C	Distinct millimeter- to centimeter-thick beds associated with other carbonate lithofacies; most abundant on inner ramp	Massive or wispy laminated, graded	Sand-sized intraclasts, partly elongate or irregular with micritic rim; silt- to sand-sized peloids, some sand-sized ooids and oncoids, rare aggregate grains; ooids and oncoids with brickwork-texture, layers often spalled off; finely to medium crystalline dolomite, idiotopic to xenotopic texture	Primary wackestones and packstones; oncoids mostly associated with stromatolites; intercrystalline and intragranular porosity
LF 10 Intraclastic breccia Fig. 11D	Millimeter- to centimeter-thick beds associated with other carbonate lithofacies, notably LF 4 and LF 6; most abundant on inner ramp	Massive	Poorly sorted, angular and flat dolostone clasts in fine dolomite matrix; clasts faintly laminated to massive	

ing sections describe the vertical facies succession and the main characteristics of each lithofacies, followed by an interpretation of depositional processes and environments.

An irregular, sharp surface separates the A4E from the overlying basal A4 tuff (LF 2); the surface is used as a datum for all studied wells (Figs. 4 and 5; Schröder et al., 2003). Up-section, carbonate content and degree of lamination increase, and the tuff grades into flat laminites. Flat and crinkly laminites together form a uniform outer ramp package without significant lateral facies variation in the studied cores (LF 3 and 4; Fig. 5).

Towards the top of the outer ramp succession, intercalations of massive dolostones become more abundant (LF 5; Figs. 4 and 5) and produce a gradual transition to the overlying massive dolostones of the middle ramp. Further up-section, massive dolostones gradually pass to laminated dolostones (LF 6; Figs. 4 and 5). Thickness and lithofacies character of massive and laminated dolostones remain constant between wells.

The first appearance of cross-laminated dolostones (LF 7) marks the base of the inner ramp. In contrast to the underlying environments, the inner ramp exhibits high variability defined by common alternations of various lithofacies (Fig. 5). Deposits of the inner ramp are dominated by laminated and massive dolostones, but intercalations of cross-laminated dolostones, dolarenites, and intraclastic breccias gradually increase up-section (Fig. 5). Very shallow deposits with indicators of peritidal deposition and exposure are absent until the topmost 5–15 m of the A4C, which are dominated by stromatolites (LF 8; Figs. 4 and 5).

Near the top of the A4C, stromatolites are interstratified with beds of nodular mosaic anhydrite (LF 1), and the A4C passes gradually to anhydrite and ultimately halite of the A5 evaporite unit (Fig. 5; Schröder et al., 2003).

3.2. Evaporite–carbonate transition

3.2.1. Anhydrite (LF 1)

The anhydrite units both underlying and overlying the A4C typically contain palmate nodules with laminar chevron inclusions of dolomite (Table 1; Schröder et al., 2003). These structures are characteristic for anhydrite pseudomorphs after selenitic gypsum, which typically forms in shallow gypsum salinas (Fig. 4; Schreiber and Kinsman, 1975; Schreiber, 1978).

3.2.2. Volcanic tuff (LF 2)

The tuff overlies the A4E anhydrite with a sharp irregular surface (Figs. 4, 5 and 6A). The rock consists of siliciclastic and volcaniclastic grains and authigenic phases (Table 1). Sedimentary structures include rare desiccation cracks (Fig. 6B) and a few skeletal halite casts.

Zircons in the tuff have a volcanic origin and were dated at 542.0 ± 0.3 Ma (Amthor et al., 2003). The angular nature of all grains indicates limited aquatic transport. Thus, the rock is interpreted as an air fall volcanic tuff with admixed windblown detrital grains. The irregular base of the tuff represents corrosion of the underlying evaporites during flooding of the basin (Figs. 5 and 6A; Schröder et al., 2003). Corrosion was accompanied by collapse of insoluble tuffaceous material into the depressions and resulted in the chaotic and mottled fabric, as was observed in modern environments (Fig. 6A; Lowenstein and Hardie, 1985; Smoot and Castens-Seidell, 1994). Early diagenetic authigenic phases further disrupted the sediment and suggest that salinity in pore waters periodically reached high levels. Modern analogs for such sediments form on the surface of sabkhas and playas (e.g., saline mudflats), as well as in the shallowest part of salinas (Smoot and Castens-Seidell, 1994). The tuff was therefore deposited on a sabkha or playa surface, whereas in-situ deformation in the saline environment occurred during or shortly after tuff deposition.

3.3. Outer ramp facies

3.3.1. Flat laminite (LF 3)

The distinguishing feature of flat laminites is their millimeter-scale planar and laterally continuous lamination that is reminiscent of varves (Fig. 7A). Laminae are (1) essentially pure finely crystalline dolomite, or (2) dolomite with 40–50 vol.% of anhydrite (Fig. 7B and Table 1).

Pairs of dolomite–anhydrite, or dolomite–dolomite laminae define couplets 1–3 mm thick. In each core,

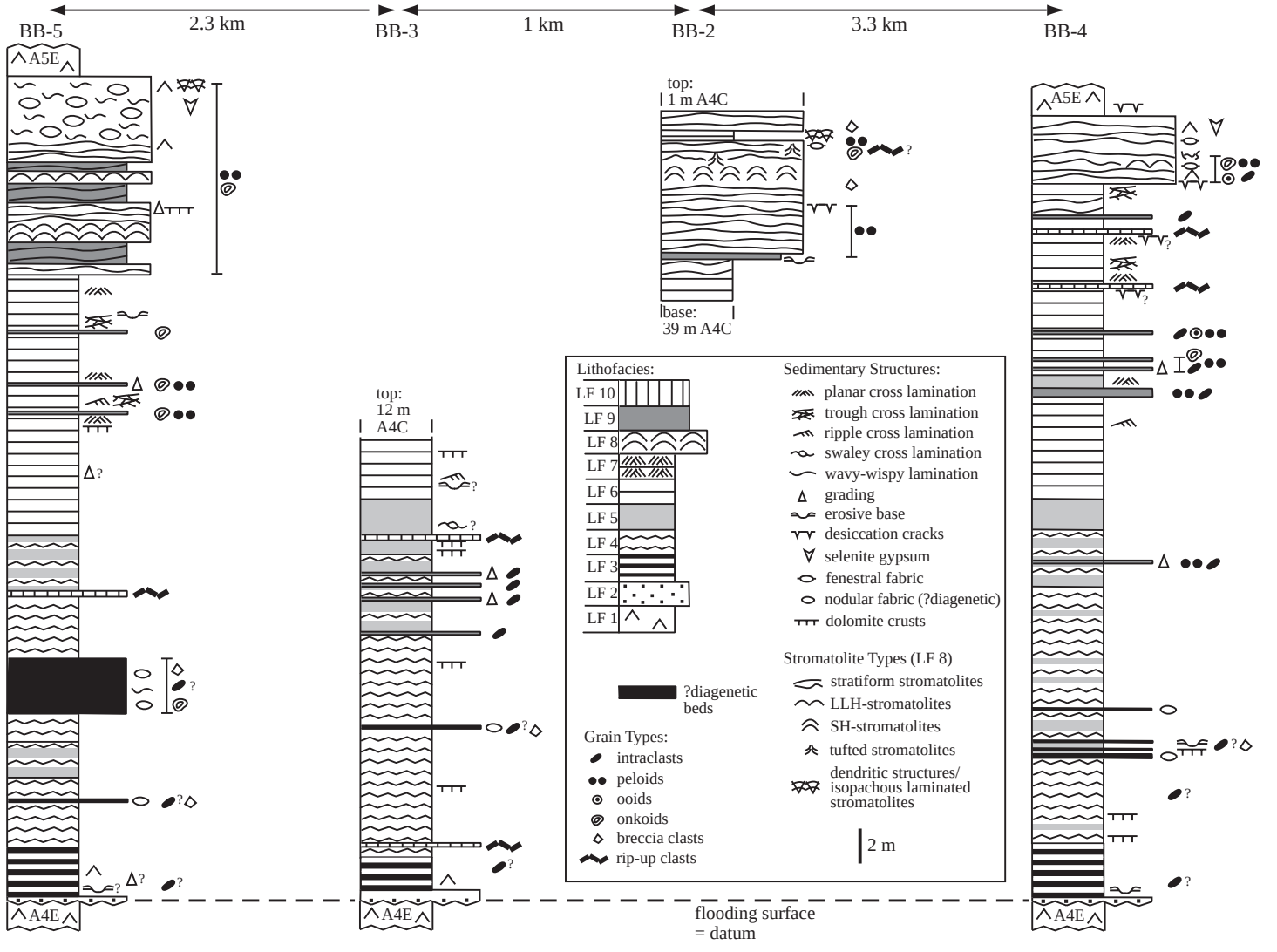

Fig. 5. Sedimentologic sections of the studied cores. Columns show the lithofacies, whereas symbols refer to additional sedimentary structures and the observed grain types. See Fig. 3A for location of wells.

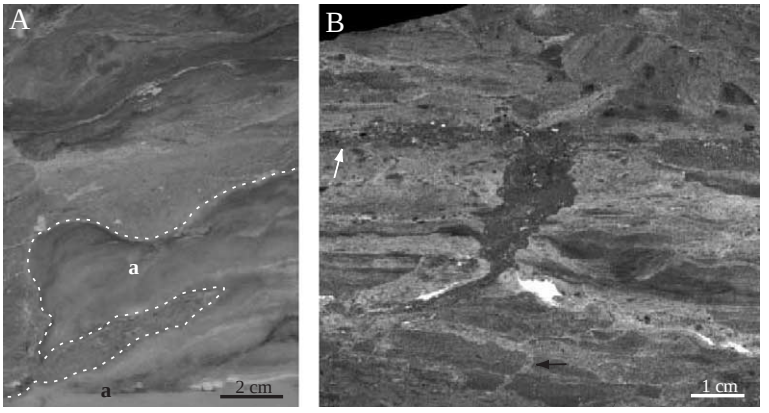

Fig. 6. Anhydrite and volcanic tuff. (A) The dashed line marks the sharp irregular contact between anhydrite (a) and the tuff. The volcanic tuff is massive at its base, while the top shows the characteristic mottled fabric, marked by dark and light streaks. The elongate area of tuff near the base could represent an injection feature into semi-consolidated sulfate sediment. Well BB-3, depth 9619′. Slabbed section. (B) Detail of the volcanic tuff with disrupted lamination at the base (black arrow), and a prominent desiccation crack in the center of the photograph. Fine-sandstone material derived from the overlying lamina fills the crack (white arrow). The upper part of the sample is characterized by a massive to mottled/nodular fabric. Well BB-5, depth 9999′. Slabbed section.

dolomite–anhydrite couplets occur in the lower part of the flat laminite interval. Transitions between these laminae are commonly gradual and are determined by variations in the anhydrite contents (Fig. 7A and B). Up-section, the anhydrite laminae gradually disappear and they are substituted by organic-rich dolomite laminae, giving rise to dolomite–dolomite couplets. Variations in organic matter contents and dolomite crystal size define the transitions between individual dolomite laminae (Fig. 7A and B).

The varve-like flat laminites are interpreted to record dominant rainout of fine carbonate and sulfate minerals in relatively deeper parts of the platform (Fig. 4). Previous authors have used finely crystalline dolomite as an indicator for abundant nucleation sites in fine precursor sediment (e.g., Murray and Lucia, 1967; Sibley and Gregg, 1987), although additional factors can complicate this relationship, such as the ratio between nucleation rate and growth rate (Sibley and Gregg, 1987), or the observation of multiple dolomite generations even in fine dolomite (Jones, 2005). It is therefore difficult to estimate grain size of the original sediment in the present case, but the detailed preservation of finely laminated fabrics indicate a fine-grained, possibly muddy, precursor.

Gradual variation of anhydrite content between laminae suggests that sulfate crystals formed in the water column (probably as gypsum, but now replaced by anhydrite) and then rained down on the sea floor forming a crystal cumulate (Fig. 7B), similar to the Permian Castile Formation (cf. Anderson et al., 1972). In the Ara Group, sulfate beds were reworked sometimes, transported down slope by gravitationally driven currents, and deposited as thin layers with an erosive base. As sulfate deposition was controlled by salinity, the dolomite–anhydrite couplets represent a phase when salinity in the water column cyclically reached sulfate supersaturation. During subsequent basin evolution, salinity remained largely normal marine and dolomite–dolomite couplets formed instead.

Shallow-water indicators, such as traction deposits with shallow-water components, desiccation cracks or stromatolites, are absent over a thickness of 2–3 m (Fig. 5). Analogous to other varved deposits, the flat laminites were deposited in relatively deep water (tens to hundreds of meters; cf. Anderson et al., 1972).

3.3.2. Crinkly laminite (LF 4)

The millimeter-scale, laterally continuous lamination in crinkly laminites is very similar to that in flat laminites (Table 1). Dark organic-rich and light organic-poor dolomite laminae form couplets (Fig. 7C). The dark laminae are characterized by small irregularities (“crinkles”; Fig. 7D). The light laminae typically fill the small depressions between the high points in the dark laminae (Fig. 7D). Dark laminae

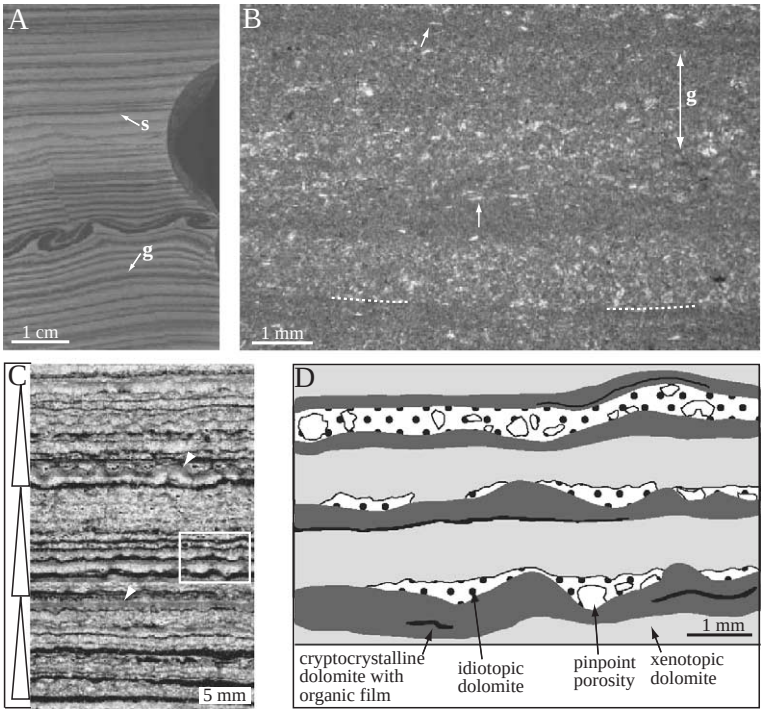

Fig. 7. Flat and crinkly laminites. (A) Flat laminites with continuous lamination. Dark laminae are composed of dolomite and anhydrite, whereas lighter laminae are almost pure dolomite. Contacts can be sharp (s) or gradational (g). Synsedimentary deformation of anhydrite-rich lamina occurs in the lower half. Well BB-3, depth 9617′. Slabbed section. (B) Photomicrograph of flat laminites showing alternating dolomite (dark) and anhydrite (light, speckled) laminae. Many anhydrite crystals are elongate flakes (arrows). Note faint grading of anhydrite crystals in upper half (g) and relatively sharp base of anhydrite-rich lamina at the bottom (dotted lines). Well BB-4, depth 9679′. Cross-polarized light. (C) Crinkly laminites with organic-rich dolomite (dark) and detrital laminae (light). Arrows point to thin recrystallized zones within detrital laminae that represent dolomite crusts. Triangles at left show centimetric cycles, each with thick organic-rich laminae at the base and thicker detrital laminae towards the top. Rectangle indicates area sketched in panel (D). Well BB-3, depth 9606′. Slabbed section. (D) Detailed sketch of the area outlined by white rectangle in panel (C). Organic-rich laminae commonly have a flat base and an irregular top, while the relief is filled up by detrital laminae. Note different dolomite crystal textures in detrital laminae, and the pinpoint porosity at the base of individual laminae.

usually have low porosity. A combined vuggy pinpoint and intercrystalline pore system in the light laminae shows high porosity (≥10%) and moderate permeability (≤120 mD) (Fig. 8). Aggrading dolomite recrystallization tends to produce a coarser xenotopic dolomite texture with a concomitant decrease in reservoir quality (Schröder, 2000). Some of the coarser dolomites contain greenish fluorescent fluid inclusions that possibly contain immature organic matter or hydrocarbons (Mattes and Conway Morris, 1990).

Crinkly laminite couplets typically are arranged in 1- to 2-cm-thick cycles (Fig. 7C). At the base of each cycle, the dark laminae are relatively thick and have a high relief. Towards the cycle tops, thickness and relief are reduced progressively while the light laminae become thicker. Dolomite crystals tend to be more xenotopic than in the thinly laminated crinkly laminites, and they have a dominantly intercrystalline pore system (Fig. 8). Whereas porosity is still comparable to that in thinly laminated couplets (≤10%), permeability is reduced (≤50 mD) (Fig. 8). Towards the top of the crinkly laminite unit in each core, the proportion of light laminae increases at the expense of organic laminae. This trend parallels the increase in distinct beds of massive dolostones (Fig. 9A).

Each couplet of crinkly laminites is interpreted to reflect accumulation of carbonate with planktonic organic matter in the dark laminae, alternating with accumulation of detrital carbonate derived from shallower parts of the platform (Fig. 7C and D). Dolomite

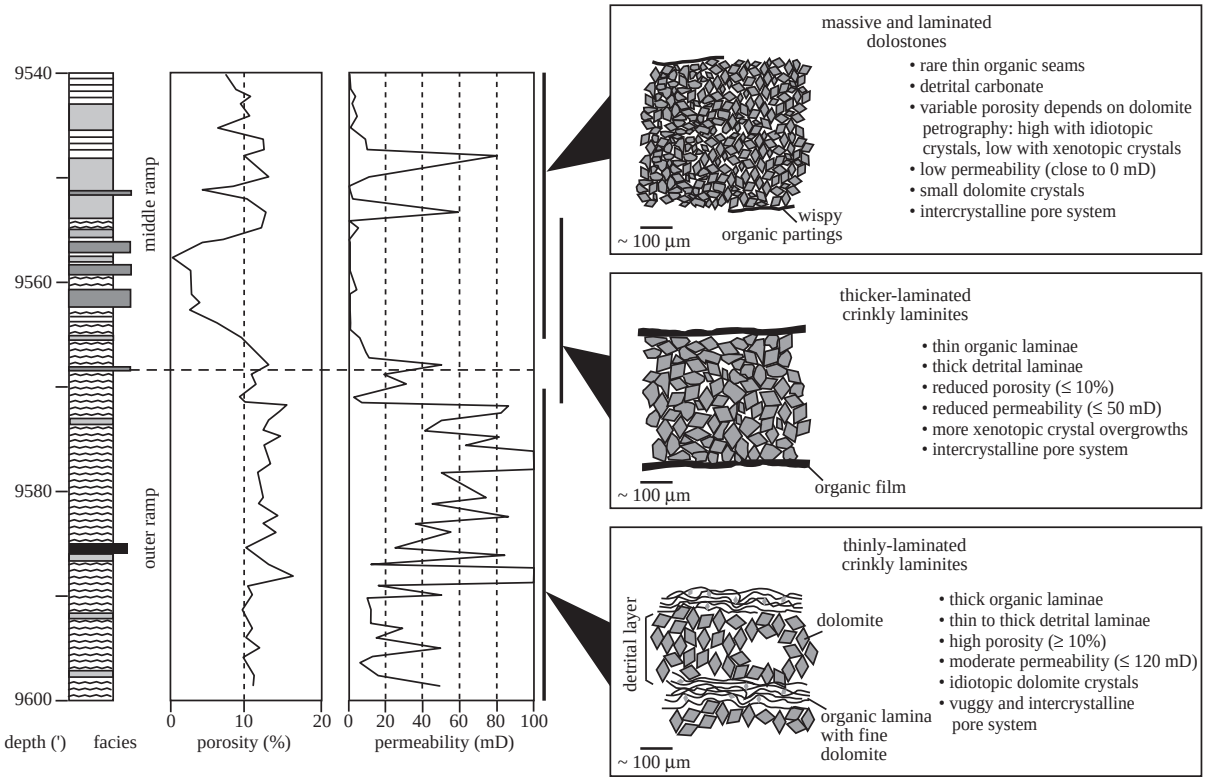

Fig. 8. Porosity and permeability data for well BB-3; data are derived from core plugs. The corresponding sketches of microfacies in crinkly laminites and massive dolostones illustrate the variation in reservoir properties. For lithofacies symbols refer to Fig. 5. See text for discussion.

crystal size and fabric preservation both argue for a fine-grained precursor (see flat laminites above). Graded deposits are suggested by the vertical crystal-size variation in some laminae. The positive relief of several laminae, and in particular those discontinuous laminae with lenses of coarser sediment, suggests an additional, but minor development of benthic microbial mats that formed upright structures and which were able to trap and bind sediment (e.g., Grotzinger and Knoll, 1999). However, there are no definitive stromatolites—domes and columns of any size are absent over the entire thickness of crinkly laminites. Depending on water depth, these mats may have been photosynthetic or possibly chemoautotrophic, such as the mats covering the sub-photic sea floor in the upwelling zones off Chile, Peru and Namibia (Gallardo, 1977; Schulz et al., 1999).

The relationship between background sedimentation and organic matter accumulation can be explained by one of two possible models: (1) intermittent periods of low to no flux of suspended fine-grained carbonate allowed the accumulation of planktonic organic matter and, to a lesser degree, the establishment of benthic microbial mats, or (2) constant, but low background flux of suspended fine-grained carbonate with intermittent planktonic and benthic blooms. Intermittent and low-volume sedimentation events prevented swamping of the thin organic-rich laminae by detrital carbonate (cf. Grotzinger and Knoll, 1999). Longer term changes in the relative balance between the two sediment sources helped control the formation of centimeter-scale cycles (Fig. 7C).

The lamination character, its lateral persistence between wells, the absence of any shallow-water structures like mudcracks or stromatolites, and the absence of indicators for shallow-water flow like ripples or lenticular bedding, all argue for deposition in relatively deep water (tens to hundreds of meters; Fig. 4). In addition, crinkly laminites occur near the

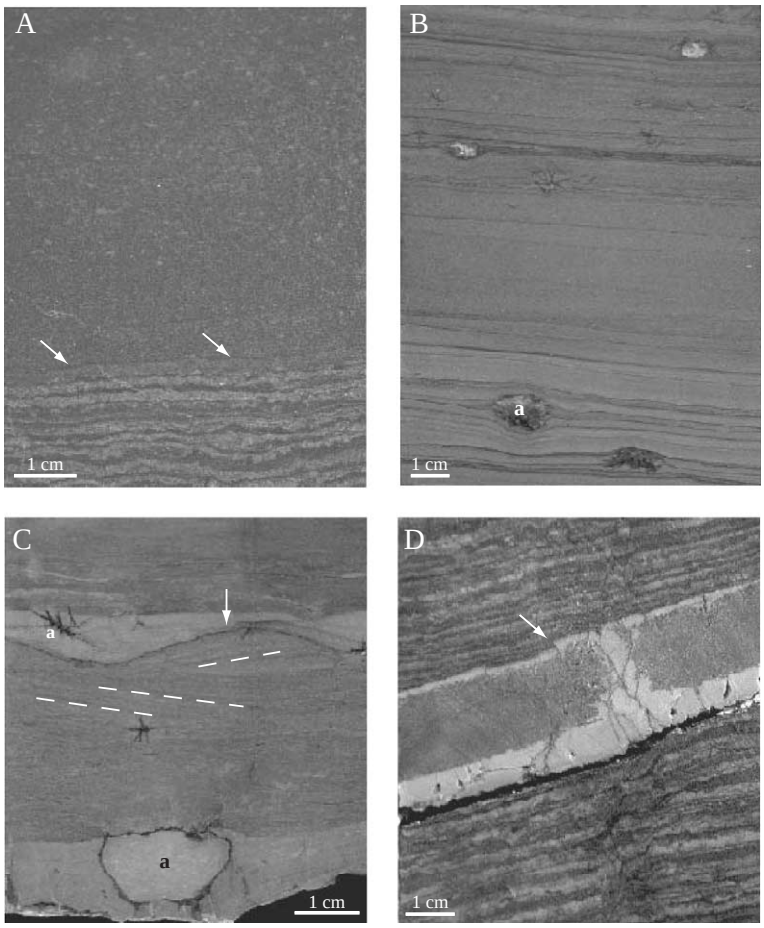

Fig. 9. Fine-grained carbonates. (A) Massive dolostone overlies crinkly laminites with a sharp contact (white arrows). Speckled fabric derives from variations in dolomite crystal size that might reflect former grains. Well BB-3, depth 9559′. Slabbed section. (B) Laminated dolostone with pre-compactional anhydrite nodules (a). Dark seams partly consist of solution seams. Well BB-4, depth 9601′. Slabbed section. (C) Laminated dolostone with faint planar cross-lamination. The irregular surface (arrow, with small stylolite) might represent an erosion surface. Anhydrite occurs as small clusters of laths or as nodules (a). Well BB-5, depth 9889′. Slabbed section. (D) Massive dolostone intercalated with crinkly laminites. The marginal zone of the dolostone was recrystallized and transformed into a low-permeability cream-colored dolostone. This alteration was a synsedimentary to very early diagenetic process related to early lithification, as suggested by the common fracturing of such beds (white arrow). Well GHF-1, depth 4345 m. Slabbed section. Sample taken from A3C, about 50 km southwest of Birba area.

base of a gradual succession of facies with increasing clastic carbonate and shallow-water structures (Fig. 4). Older Ara Group cycles show a very similar vertical facies stacking with basal crinkly laminites, but in these cases, a lateral transition between crinkly laminites and an equivalent shallow-water facies could be demonstrated (Grotzinger and Amthor, 2002). Periodically, slumping and incipient brecciation occurred, perhaps induced by slope creep, tectonic activity, gas escape or periodic storm activity.

3.4. Middle ramp facies

3.4.1. Massive dolostone (LF 5)

Beds commonly are massive, though wispy organic partings can create faint lamination (Fig. 9A and Table 1). Whereas massive dolostones are petrographically similar to detrital laminae of underlying crinkly laminites, dolomite crystals commonly are smaller in massive dolostone (Fig. 8). Highest porosities are associated with idiotopic dolomite texture and permeability is generally low (Fig. 8).

3.4.2. Laminated dolostone (LF 6)

This lithofacies is very similar to massive dolostone, the main difference being the development of a distinct millimeter- to centimeter-scale lamination (Fig. 9B). The lamination is created by flat and wavy organic and stylolitic partings, the latter probably following a primary organic lamination (Fig. 9B). Graded crystal size may also indicate grading in the original sediment.

For massive and laminated dolostones, the extent of dolomitization and fabric destruction prevents firm identification of grain size in the precursor sediment. Based on the petrographic characteristics and the similarity with detrital laminae in crinkly laminites, it was possibly relatively fine-grained (mud ± silt) and accumulated below fair-weather wave-base. Erosive surfaces suggest limited reworking and transport. The position of these two lithofacies in the gradual transition from an environment with low to intermittent sedimentation rates (crinkly laminite) to persistent reworking in relatively shallow water (cross-laminated dolostone) suggests a gradual increase in sediment export from shallower parts of the ramp. In summary, massive and laminated dolostones probably represent a combination of hemipelagic deposition of suspended carbonate (massive beds, in particular the interbeds in crinkly laminites), fine-grained turbidites and/or tempestites (graded beds, some with erosive bases) and possibly fine-grained debris flows (Fig. 4; cf. Cook and Mullins, 1983; Pelechaty et al., 1996). There is however no sedimentary evidence for storms impinging directly on the sea floor.

3.5. Inner ramp

3.5.1. Cross-laminated dolostone (LF 7)

Cross-lamination includes small-scale ripples, planar and low-angle trough cross-lamination (Fig. 9C and Table 1), as well as poorly defined swaley cross-lamination. Scoured surfaces occur locally at the base of cross-laminated beds. The microfacies is similar to that of massive and laminated dolostones.

Traction currents, probably associated with waves, deposited the cross-laminated dolostones (cf. Burchette and Wright, 1992). Although poorly preserved, the swaley cross-lamination suggests the occurrence of storms (e.g., Southard et al., 1990). The environment was above fair-weather wave-base (Fig. 4). Cross-lamination requires a grain size coarser than mud (i.e., >20 μm), and so these rocks are interpreted to have been silt- to fine sand-sized carbonate.

3.5.2. Stromatolites (LF 8)

Stromatolite morphologies include (1) stratiform (Fig. 10A); (2) domal (LLH- and SH-types of Aitken, 1967); (3) columnar-tufted (Fig. 10B); (4) dendritic and chevron structures (Fig. 10C); and (5) isopachous (Fig. 10D). Types 1–3 contain common sheet-like intercalations of dolarenites (LF 9) and massive dolostones (LF 5) (Fig. 5). Desiccation cracks and fenestrae occur in association with the more columnar-tufted morphologies. Stromatolites usually are altered; their microfabric contains micritic to coarsely crystalline dolomite, abundant evaporite cements and replacements, coarse calcite and minor chert.

The discontinuous lamination of the observed stromatolites is consistent with formation by trapping and binding (Fig. 10A; cf. Black, 1933; Grotzinger and Knoll, 1999). Stratiform to domal stromatolites commonly lack emergence indicators such as desiccation cracks or fenestral fabrics and, therefore, probably formed in shallow subtidal environments. Fenestral and tufted stromatolites contain desiccation cracks, consistent with formation in very shallow environments subject to periodic exposure (Figs. 4 and 5; cf. Hardie and Ginsburg, 1977). The assemblage of stromatolites and dolarenites with shallow-water grains indicates an environment subject to constant agitation. Evidence for prolonged peritidal deposition is absent (e.g., there are no peritidal cycles with exposure caps).

The dendritic structures may be explained by one of two possible models. First, the contained chevron structures are similar to laminar chevron inclusions of detrital sediment in selenitic gypsum (Schreiber and Kinsman, 1975; Schreiber, 1978). This similarity suggests bacterial breakdown of gypsum, which resulted in elevated bicarbonate concentrations and carbonate precipitation (e.g., Decima et al., 1988). In an alternative model, the dendritic fabrics resemble tufa structures that are described from recent to Precambrian tidal flats (e.g., Hardie, 1977; Pope and Grotzinger, 2000), and from terrestrial environments (e.g., Chafetz and Folk, 1984; Demicco and Hardie, 1995). Such tufas commonly form by direct precipitation in a mineralizing system, possibly

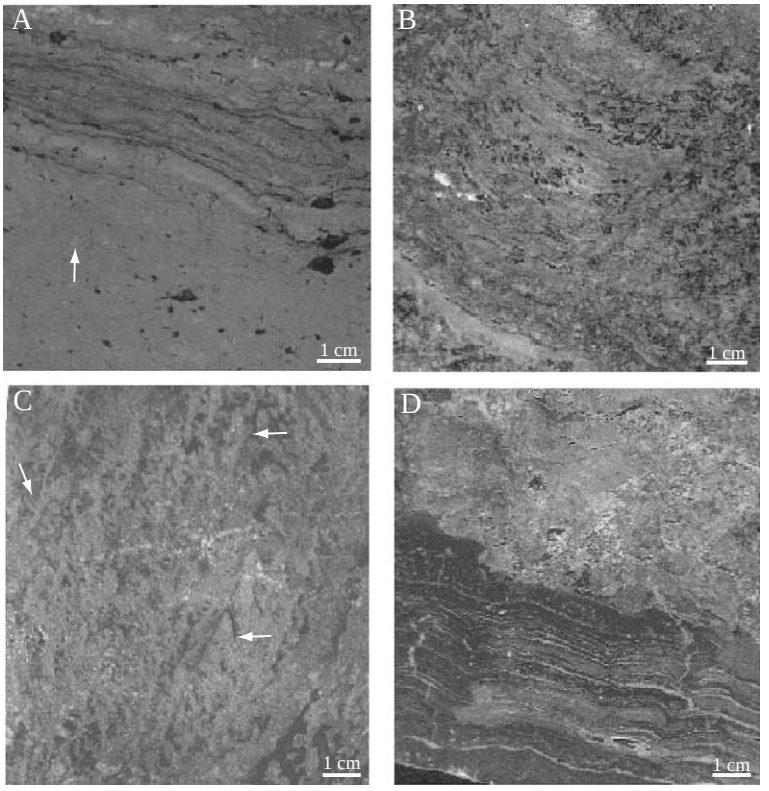

Fig. 10. Stromatolite types. (A) Stratiform stromatolite (upper half) overlying a massive dolostone. Discontinuous lamination, often with stylolites, is typical of stromatolites formed by trapping and binding. Lighter specks in the massive dolostone could indicate recrystallized grains (e.g., arrow, compare Fig. 9A). Dark blebs are anhydrite. Well BB-4, depth 9541′. Slabbed section. (B) Strongly recrystallized tufted stromatolite with concave-up laminae. Stromatolite incorporates abundant recrystallized grains, mainly ooids and oncoids. Well BB-2, depth 9289′. Slabbed section. (C) Dendritic structures (arrows) with laminar chevron structures. Well BB-5, depth 9844′. Slabbed section. (D) Sample with isopachous stromatolite at the base. Irregularities are propagated through the complete section. Stromatolite is overlain by strongly recrystallized and brecciated dolostone. This association is the first evidence for deposition under restricted conditions and elevated salinity (cf. Pope et al., 2000). Well BB-2, depth 9287′. Slabbed section.

mediated by microorganisms (Chafetz and Buczynski, 1992; Grotzinger and Knoll, 1999). In the A4C, direct precipitation of such carbonate fabrics would have been coupled to the observed increase in salinity. Isopachous stromatolites represent a similar environmental setting (Fig. 10D; see Pope et al., 2000).

3.6. Associated lithofacies

3.6.1. Dolarenite (LF 9)

Dolarenite beds are graded to massive and contain silt- to sand-sized grains (Fig. 11A–C and Table 1). Grain composition varies with stratigraphic position: Arenites in lower parts of the studied section are composed mostly of intraclasts and some peloids. Up-section, peloids and intraclasts are commonly associated with ooids and oncoids (Fig. 11A and B). Elongate intraclasts with a micritic rim are common (Fig. 11C). Porosity ranges up to ~10%, whereas permeability generally remains below 10 mD.

Based on the presence of grains, dolarenites had wackestone and packstone precursors. Some could have been grainstones, where finer material was winnowed. These rocks were deposited as subtidal sheets of carbonate arenites that were subject to repeated reworking by unidirectional and oscillating currents and waves (Fig. 4). The graded beds may represent gravitational settling of sediment from turbid storm- or slope-induced flows (cf. Cook and

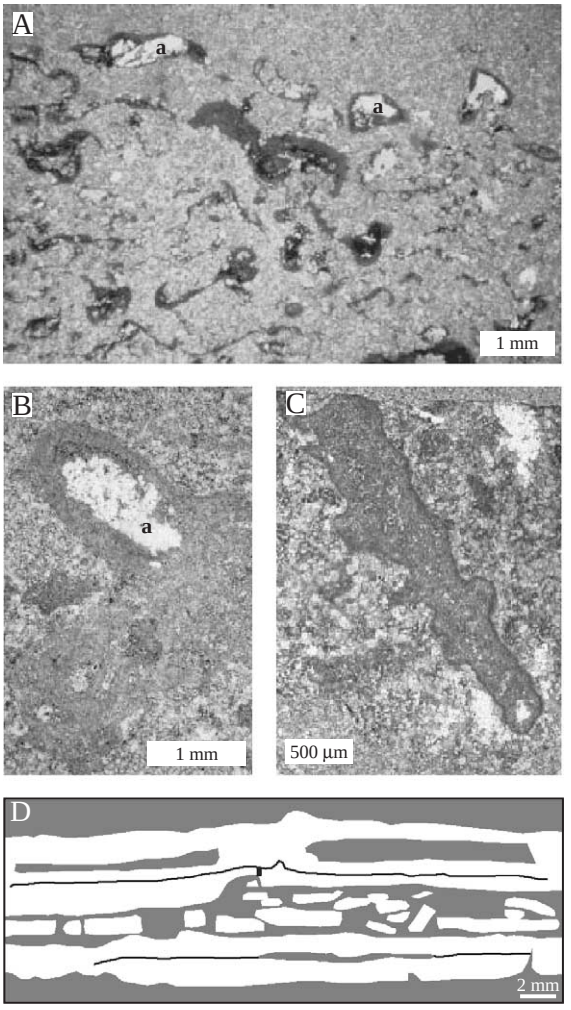

Fig. 11. Carbonate grains. (A) Dolarenite bed overlain by massive dolostone at the top. Grains consist of deformed and hook-shaped intraclasts, some with internal lamination reminiscent of ooids. Note common intragranular anhydrite cement (a). Well BB-4, depth 9572.5′. Photomicrograph, plain polarized light. (B) Aggregate grain with several ooids and intragranular anhydrite cement (a). Well BB-4, depth 9542′. Photomicrograph, plain polarized light. (C) Elongate intraclast with irregular outline and micritic rim. Well BB-4, depth 9542′. Photomicrograph, plain polarized light. (D) Thin intraclastic breccia sheet within crinkly laminites. Grey: finely crystalline dolomite of detrital lamina; white: organic lamina recrystallized to cream-colored dolostone; black lines: remains of organic film. Well BB-5, depth 9941′.

Mullins, 1983; Aigner, 1985; Aurell et al., 1998). The vertical trend in grain composition is consistent with overall shoaling of the platform and an increased proportion of shallow-water grains. Elongate intraclasts and chips may be derived from the localized reworking of microbialites and fine-grained laminated carbonates. Irregular grains with a micritic rim resulted from boring by endolithic microbes, although other processes, such as micrite recrystallization, could have contributed as well (Fig. 11C; cf. Reid and Macintyre, 2000).

3.6.2. Intraclastic breccia (LF 10)

Breccia beds are massive and contain poorly sorted, angular and flat dolostone clasts in a fine dolomite matrix (Fig. 11D). The internal fabric of clasts is faintly laminated to massive and clast lithofacies usually matches the surrounding rock. All stages from in-situ breccias with a fitted fabric, to transported breccias were observed, but in-situ brecciation is relatively rare.

In upper parts of the A4C, cracked, laminated dolostones and intraclastic breccias are commonly associated in centimeter-scale units. Within each unit, cracking and in-situ brecciation of laminated dolostones increase up-section, and an intraclastic breccia caps the unit.

Breccia units may be the result of evaporite dissolution, exposure, reworking by storms and waves, or gravity transport, all of which would have affected at least partially lithified sediments (cf. Demicco and Hardie, 1995). Evaporite dissolution collapse is possible only for in-situ breccias with little matrix, whereas breccias associated with the deeper water crinkly laminites seem to be mostly gravity-transported. Breccias of the inner ramp are related to exposure, storms and/or waves. In particular, the sequence of beds with up-section increase of brecciation may represent upward shoaling to the zone of wave or storm reworking. Storm- and wave-induced cyclic loading can act repeatedly on partly lithified sediment, with the result that internal pore pressure may build up and ultimately cause cracking of the sediment (Suhayda, 1977; Cowan and James, 1992).

4. Reservoir diagenesis

Porosity and permeability data, derived from neutron and density logs and from core plugs, have been used to subdivide the A4C into three reservoir units

with a remarkably uniform distribution across the platform (units A–C in Figs. 4 and 12; Mattes and Conway Morris, 1990; Schröder, 2000). Reservoir quality is strongly dependent on facies, and the three reservoir units roughly correlate with inner, middle and outer ramp facies (Fig. 12). Unit A contains outer ramp laminites; the porosity ranges from 0.4 to 23.0%, whereas permeability is between 0.01 and 313.0 mD. The crinkly laminites represent the main flow unit of the A4C. Reservoir unit B encompasses facies of the middle ramp and part of the inner ramp (Fig. 12). Porosity varies from 0.7 to 15.5% and permeability ranges from 0.01 to 80 mD. At its base, the vertical transition from crinkly laminites to massive dolostones is characterized by an increase in detrital, possibly fine-grained carbonate at the expense of organic material, and a decrease in permeability that is more pronounced than the parallel decrease in porosity (Fig. 8). Unit C shows reservoir development in inner ramp stromatolite and thrombolite buildups and carbonate arenites. Porosity values are between 0.1 and 21.2%, and permeability varies between 0.01 and 170 mD. Much of the porosity in the A4C is intercrystalline and associated with relatively fine (earlier) idiotopic dolomite, whereas coarse late diagenetic dolomite and calcite replacements and cements tend to destroy reservoir quality (Mattes and Conway Morris, 1990; Schröder, 2000). Anhydrite and halite cements (Fig. 11A and B), pre-compactional anhydrite nodules (Fig. 9B) and the replacement of carbonate by evaporites were commonly observed throughout the A4C. The detrimental effects of evaporites on reser-

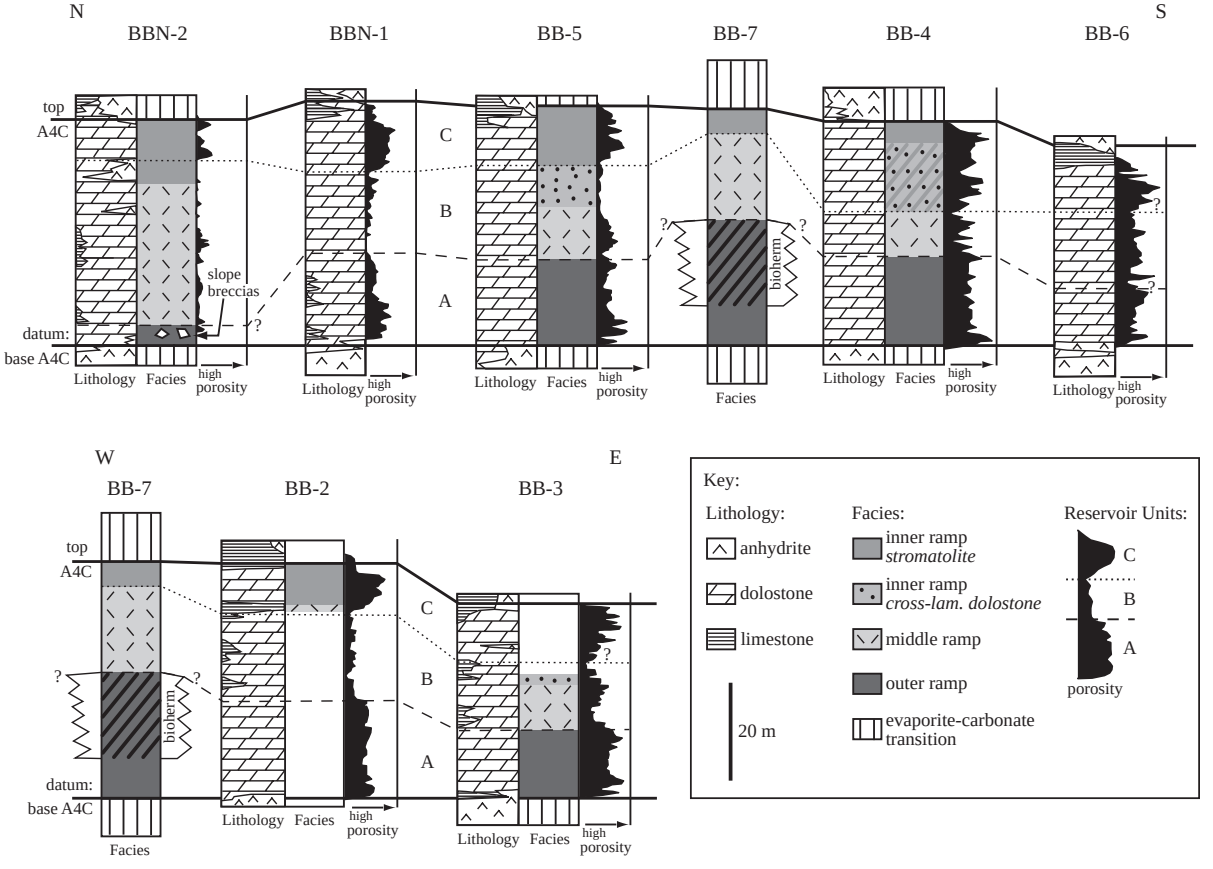

Fig. 12. North–south (top panel) and west–east (bottom panel) cross-sections of the Birba platform showing lithology, facies and reservoir units of key wells used in the study. Lithology represents a close estimate of true lithology distribution in the sections and is derived from data collected during drilling. Facies interpretation is based on core descriptions in all wells except BB-7 where FMI™ (FormationMicroImager) logs were used. These logs provide an image of resistivity distribution. Reservoir units were calibrated with lithofacies.

voir quality are best documented by the evaporite "cap" at the top of the A4C, where porosity and permeability drop off rapidly with an increase in diagenetic evaporites (Fig. 4).

In summary, three key diagenetic controls on reservoir quality in the A4C can be identified: generation and preservation of early idiotopic dolomite, low permeability in fine-grained carbonates, and the presence of evaporites. Diagenesis of the A4C will be discussed briefly to provide a context for these factors.

Pervasive dolomitization was the principal diagenetic event in the A4C, usually followed by evaporite cementation and replacement to various extents (Mattes and Conway Morris, 1990; Schröder, 2000). Locally, dolomite recrystallized to a coarser mosaic that destroyed depositional fabrics and further added to reservoir degradation. The early dolomite phase is attributed to reflux dolomitization (Mattes and Conway Morris, 1990; Schröder, 2000). Such a scenario is likely because dolomites are associated with thick evaporite deposits, and the abundance of evaporite cements and replacements testifies to the passage of hypersaline brines (e.g., Land, 1982). Given the organic-rich nature of the outer ramp deposits in the A4C, organogenic dolomitization (e.g., Baker and Kastner, 1981; Slaughter and Hill, 1991) may have played an additional role, although the relationship between organic matter and dolomitization of the A4C is not firmly established. However, fluorescent fluid inclusions in dolomite crystals of crinkly laminites suggest the presence in the pore system of early hydrocarbon expulsion products from the inherent organic material (Mattes and Conway Morris, 1990; Schröder, 2000). Such fluids could have delayed diagenesis, preserved early dolomite and aided in the development of crinkly laminites as the main flow unit of the A4C (Schröder, 2000).

The relationship between smaller dolomite crystal size and reduced permeability in massive dolostones relative to crinkly laminites is consistent with observations from other basins (Fig. 8; Lucia, 1995). Although the original grain size cannot be determined with certainty (see above), it is quite possible that low permeability in the fine dolomite mirrors conditions in a fine-grained precursor sediment. As a result, dolomite recrystallization should have been slow, but more importantly, the massive dolostones act as a low-permeability barrier to fluid flow at the top of reservoir unit A (Fig. 8).

Although the shallow-water facies near the top of the A4C likely had high initial porosities, these were partly degraded during diagenesis through precipitation of abundant evaporite cements and replacive evaporites, in particular in the evaporite "cap" (Fig. 4; Mattes and Conway Morris, 1990; Schröder, 2000). In addition, the grainy shallow-water facies occur as thin beds and are not sufficiently thick to act as significant flow units.

5. Discussion

5.1. Platform geometry

Key attributes of the A4C are (1) gradual transitions between relatively broad facies belts; (2) monotonous sheets of deeper water facies contrasting with a greater degree of complexity and lateral heterogeneity in shallow-water facies; (3) dominantly fine-grained carbonate with coarser grained facies tending to occur mostly in the shallowest parts of the succession; and (4) lack of a discernible break in slope. Very coarse-grained sediment is conspicuously rare in the transition zone between the outer and middle to inner ramp facies belts, which indicates a gentle depositional profile. Nevertheless, the slope breccias in well BBN-2 suggest some limited reworking and transport to deeper parts of the platform, perhaps across a step in the depositional profile (Fig. 12). Scarcity of grains points to a low-energy setting for the shallower parts of the platform. The A4C thus represents a low-energy muddy carbonate ramp (Fig. 13; see Wilson, 1975; Read, 1985).

The geometry of the Birba ramp is constrained by its relationship to the broad shelf in the west and the shelf edge in the east (Fig. 3A). The ramp most likely onlapped and was attached to the emergent high at the shelf edge (Fig. 3C). Seismic reflection data show that the A4C thins out towards the west, and we suggest a homoclinal ramp sloping away from the shelf edge in a westerly and/or northwesterly direction (Figs. 3C and 13).

It is generally difficult to define the internal geometry of thin carbonate ramps (Burchette and Wright, 1992), and the Birba ramp is no exception. The present study identified sheet-like units with minimal thickness variations across the entire Birba area

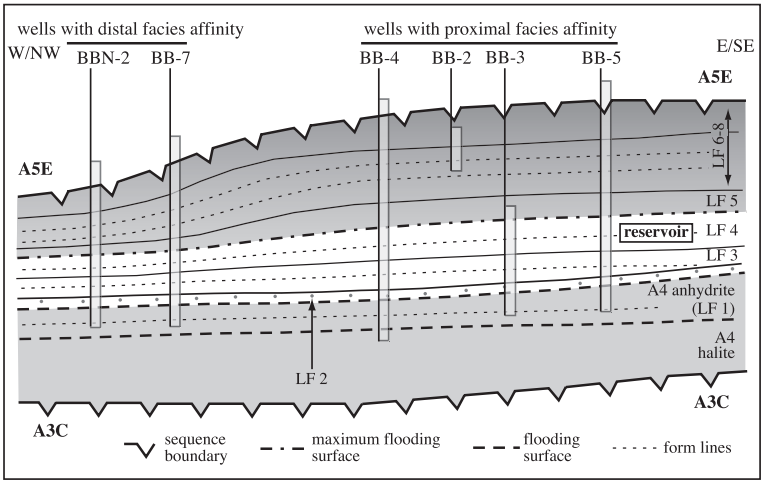

Fig. 13. Sequence stratigraphic architecture and main surfaces of the A4 evaporite–carbonate sequence. The figure also shows the main lithofacies, including the crinkly laminite reservoir facies. Wells used in this study are shown in their approximate position on the ramp, according to distal versus proximal facies affinity. Shaded boxes indicate core coverage.

(Figs. 5 and 12). All wells have the tripartite subdivision of reservoir units that were calibrated with outer, middle and inner ramp facies. Nevertheless, some general proximity trends emerge in a picture of the entire study area (Fig. 12). Thin outer ramp facies in well BBN-2 include slope breccias and are overlain by thick successions of middle ramp facies (Fig. 12). A thrombolitic bioherm was identified in well BB-7. Other authors have related the growth of such bioherms to conditions of sediment-starvation and/or more available accommodation space (Burchette and Wright, 1992; Tucker et al., 1993). In the same well, inner ramp thicknesses are reduced relative to wells farther east (Fig. 12). These observations suggest that locations in the west and northwest of the Birba ramp could have a more distal facies character, consistent with the assumption that the ramp sloped towards the west and/or northwest (Figs. 3C and 13).

This setting also explains the low-energy character of the Birba ramp. The ramp was not facing an open ocean basin. Winds were dissipated over the large and relatively shallow shelf, and by the exposed shelf edge (cf. Burchette and Wright, 1992; Aurell et al., 1998).

5.2. Depositional model and sequence stratigraphy

5.2.1. Lowstand systems tract

The thick evaporite units at the base of individual Ara cycles represent mostly accommodation minima within the South Oman Salt Basin (Mattes and Conway Morris, 1990; Schröder et al., 2003), and the A4 halite forms the LST of the A4 depositional sequence (Fig. 14). Lowstand accommodation minima alone have the potential to provide basin restriction and surface disconnection from the open ocean that are required for large-scale evaporite deposition (Tucker, 1991; Sarg, 2001). However, evaporites formed also during early transgressive and late highstand phases (see below).

5.2.2. Transgressive systems tract—evaporite–carbonate transition, outer ramp deposition

Two sharp surfaces separate A4 halite and A4 anhydrite, and A4 anhydrite and A4 carbonate, respectively (Figs. 4, 5, 14 and 15A; Schröder et al., 2003). Older evaporites are corroded along these surfaces and deep-water A4 carbonates overlie shallow-water sulfates (Fig. 6A). The surfaces thus represent flooding events at the beginning of marine transgression into the basin (Figs. 14 and 15A; Mattes and Conway Morris, 1990; Schröder et al., 2003). The anhydrite unit between these surfaces represents an early transgressive systems tract, although the water depth did not yet increase, as indicated by the preserved shallow-water selenite structures and desiccation cracks. Due to their rapid precipitation rates, sulfates were able to fill any accommodation space created during the early transgression (Schröder et al., 2003).

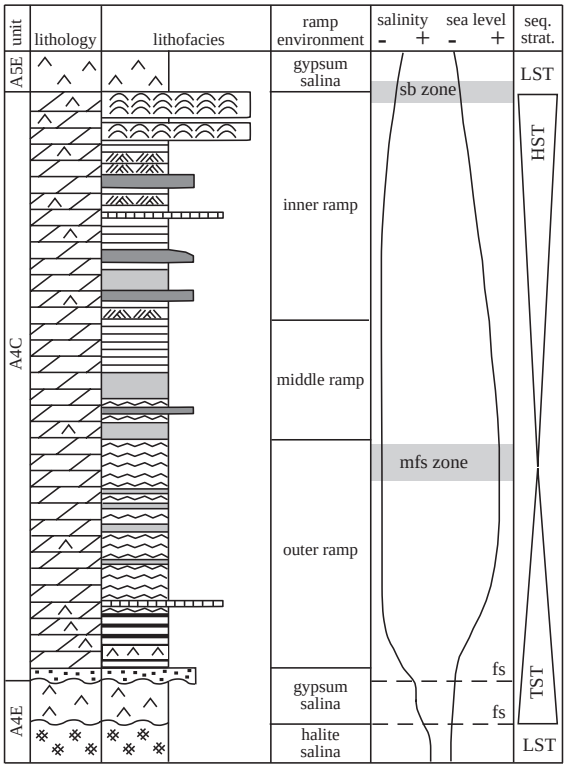

Fig. 14. Sequence stratigraphic interpretation of the sedimentary succession in the A4 carbonate. The evolution of salinity, sea level and accommodation space is shown on the right. Key surfaces are indicated (fs—flooding surface, mfs—maximum flooding surface, sb—sequence boundary). Maximum flooding surface and sequence boundary are only given as shaded bars, because the exact location of these surfaces cannot be determined with certainty (see text for discussion) (modified after Schröder et al., 2003).

Above the flooding surfaces, continued arid conditions promoted cyclically elevated salinity and the formation of flat laminites similar to the Permian Castile evaporites (Figs. 7A and 15A; cf. Anderson et al., 1972). Crinkly laminites, in contrast, record deposition under conditions of normal marine salinity (Fig. 15B). Similar laminites have been described from other evaporite–carbonate transitions and non-evaporitic settings (e.g., Davies and Ludlam, 1973; Knoll et al., 1995; Pope et al., 2000). Requirements for laminite formation are (1) minimal or absent biological and physical disturbance of sediments; (2) a stratified water body with deposition of particles from surface waters (Davies and Ludlam, 1973). The resulting depositional environments were uniform over large areas, but depositional processes alternated rhythmically to produce laminites (Davies and Ludlam, 1973).

The fine-grained carbonate of the A4C outer ramp could represent a mix of precipitated and suspended particles, the latter derived from shallow platform areas. Because there are only a few relatively thin beds of coarser facies, and clasts in these beds are commonly locally derived, it can be assumed that the shallower ramp had only limited influence on outer ramp depositional processes. Transport distances in these beds may not have been long.

With slow precipitation and gravitational settling of sulfate and carbonate minerals as the dominant sedimentation modes on the outer ramp, deposition could not keep up with the generation of accommodation space during flooding (Fig. 14). As a result of the strong subsidence in the previous evaporitic LST, the basin represented a relatively deep depression that was rapidly flooded during transgression, while carbonate production lagged behind (Kendall, 1992; Schröder et al., 2003). Near the top of the crinkly laminite unit, the onset of significant export of fine-grained carbonate from shallower parts of the ramp represents an important change in depositional processes. Accommodation space made available during the previous transgression was more rapidly filled with sediment derived from proximal parts of the platform (Figs. 14 and 15B). Because the change is gradual, a maximum flooding zone is placed close to the top of crinkly laminites (Fig. 14).

5.2.3. Early highstand systems tract—middle ramp deposition

The transition between laminites and overlying fine-grained carbonates is best accommodated in a prograding ramp model, where distal, finely laminated rocks show an upward increase in the number of interbedded massive mudstones and thin debris flow layers (Fig. 15B). These beds represent increasing sediment export from shallower parts of the platform. In this respect, the A4C is similar to the Khatyspyt–Turkut transition in the terminal Proterozoic section of the Olenek uplift, Siberia (Knoll et al., 1995; Pelechaty et al., 1996).

Middle ramp deposition occurred mostly through suspension settling during relatively quiet periods,

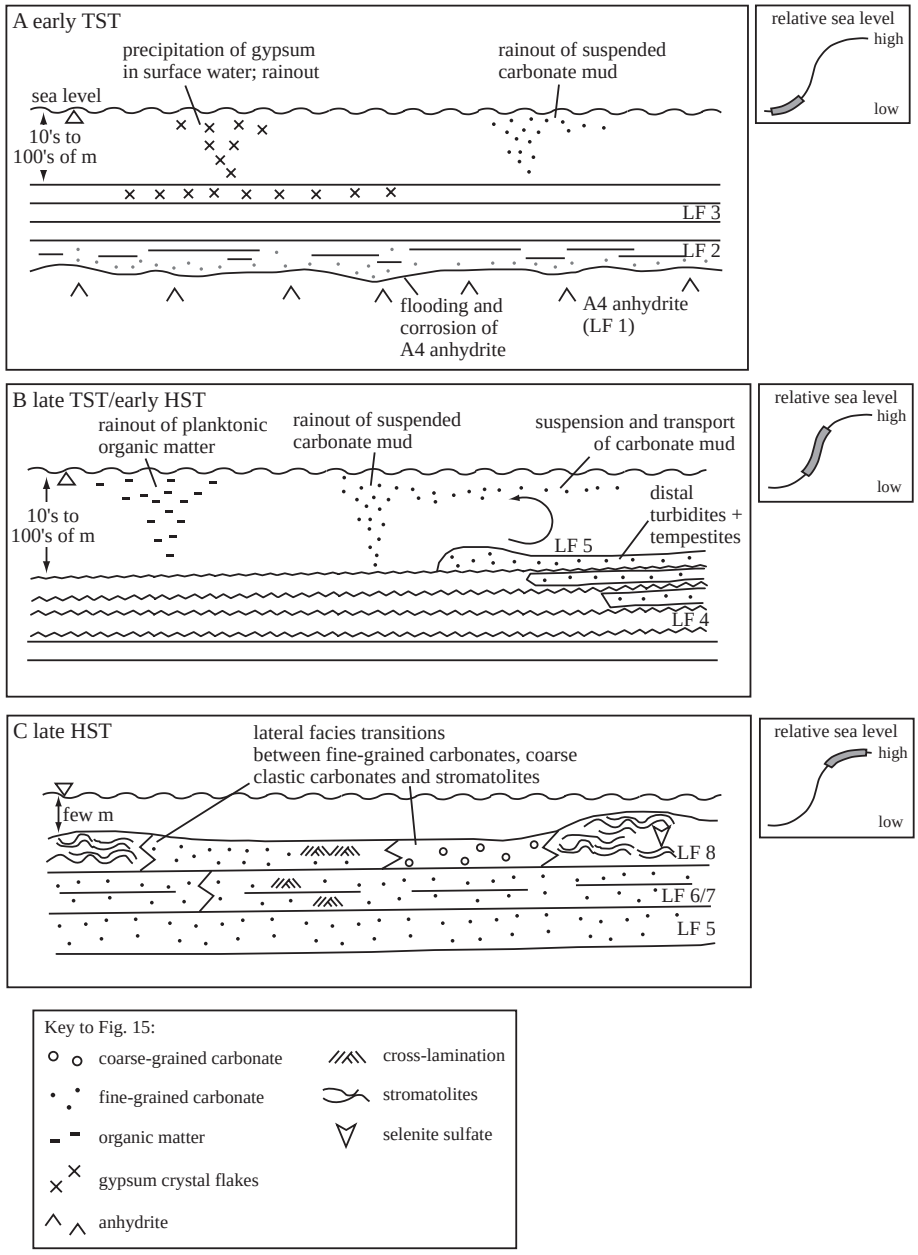

Fig. 15. Stratigraphic and depositional evolution of the A4 carbonate. Panels (A–C) illustrate the major sedimentary processes and facies deposited. Small sketches at right show evolution of relative sea level. See text for discussion.

punctuated by deposition of turbiditic beds and perhaps distal tempestites (Fig. 15B; cf. Aigner, 1985; Calvet and Tucker, 1988; Burchette and Wright, 1992). The environment was located below the fair-weather wave-base. It is, however, impossible to determine whether the transition between the outer and middle ramp of the A4C corresponds to storm wave-base (cf. Burchette and Wright, 1992), because evidence for direct storm impact on the sea floor is absent.

5.2.4. Highstand systems tract—inner ramp deposition

The first appearance of cross-lamination marks an important change in the physical processes of sedimentation, from suspension settling to traction. Deposition occurred in a subtidal environment above fair-weather wave-base (Fig. 15C). The absence of carbonate sand shoals suggests wave action was limited in frequency and/or intensity (cf. Fairchild and Herrington, 1989). Extensive tidal flats and peritidal cycles are absent, so tidal processes also had minimal influence.

Studies of other carbonate ramps have suggested relatively uniform distribution of carbonate production over most middle and inner ramp settings, with no dominant production site as in rimmed shelves (Wright and Faulkner, 1990; Elrick and Read, 1991; Burchette and Wright, 1992). This pattern is essential to maintain a homoclinal ramp profile during shallowing of the ramp (Elrick and Read, 1991). Observations from the present study are generally consistent with such a model. The limited occurrence of peritidal environments or stromatolites in the A4C suggests that shallow subtidal and peritidal carbonate production was not significantly higher than in other, deeper parts of the ramp (cf. Wright and Faulkner, 1990). Inner ramp grain types are dominantly of shallow-water origin. Although micritization of A4C grains was observed (Fig. 11C), this mechanism could not have been sufficient to generate the observed amounts of carbonate mud (Grotzinger, 1989). However, the production of mud through whitings (Shinn et al., 1989; Robbins and Blackwelder, 1992) would have been greatly facilitated by the higher saturation state of Precambrian seawater for $CaCO_3$ (Grotzinger, 1989; Tucker, 1992; Grotzinger and Kasting, 1993). In this latter mode, the mud-producing carbonate factory may have extended over almost the entire platform, except in the deepest parts where laminites accumulated under conditions of low sedimentation rate.

Spatially variable shallow-water currents were effective agents to cause redistribution and accumulation of dominantly fine-grained carbonate over the entire inner ramp (cf. Aurell et al., 1998). The heterogeneous lithofacies pattern in the shallow areas of the A4C platform represents a response to reduced rates of accommodation space creation in a highstand situation (Figs. 14 and 15C).

5.2.5. Late highstand systems tract—evaporite–carbonate transition

Interstratified anhydrite beds near the top of the A4 carbonate indicate the gradual transition from shallow-water carbonate environments to shallow-water gypsum salinas of the A5 evaporite (Fig. 14). These deposits could represent platform-wide, but short-lived events of elevated salinity, although they are difficult to correlate between wells. Alternatively, sulfate deposits may have accumulated locally in salinas behind irregular stromatolite barriers (cf. Fairchild and Herrington, 1989).

No regionally significant subaerial exposure surface is observed at the top of the A4C. As a result of the gradual facies changes, it is difficult to draw a sequence boundary between the A4 HST and the subsequent A5 evaporite, and consequently only a sequence boundary zone was defined (Fig. 14). It should be emphasized again that the A5 evaporite, like all Ara Group evaporite units, represents thick evaporite deposition across the entire SOSB. As such, it formed during a basin-wide accommodation minimum, which provided the necessary disconnection from the main water source (Fig. 14; Schröder et al., 2003). The important observation is that these LST evaporites blanket the former topographic highs like the Birba platform. This scenario is in contrast to most sequence stratigraphic models for large-scale evaporite deposition, which predict exposure of platform carbonates, while lowstand evaporites precipitate in the basin (Tucker, 1991).

Increased subsidence on the Birba platform is a likely mechanism to allow continuous evaporite precipitation in shallow salinas without significant subaerial exposure (Schröder et al., 2003). At the same time, tectonic activity caused uplift of barriers (e.g., shelf edge east of the Birba platform) and possibly an additional relative sea-level rise. Characteristic successions of stromatolites, formed by both trapping/binding and precipitation, and carbonate–evaporite laminites can be used as evidence for such a relative sea-level rise (Pope et al., 2000). For example, in well BB-2, tidal flat (?) isopachous stromatolites are overlain by facies of slightly deeper water (Figs. 5 and 10D), although this succession may simply relate to shifting tidal flats in the proximal portion of the platform. In summary, a combination of increased basin subsidence and possibly transient

flooding by high-salinity seawater caused A5 evaporite deposition *on top* of the former carbonate platform, but without a marked exposure surface between them.

5.3. Implications for reservoir quality

Sedimentary processes on the Birba ramp, sequence stratigraphy and diagenesis have important implications for reservoir characteristics. Reservoir unit C contains relatively porous shallow-water facies with good reservoir potential (Fig. 4). However, its position directly below the A5 evaporite resulted in degradation of reservoir quality through evaporite precipitation (Fig. 4).

In reservoir unit A, the distribution of fine-grained carbonate and organic material had an impact on reservoir quality of crinkly laminites. Here, organic material accumulated during a time of reduced flux of clastic carbonate. The presence of organic material possibly influenced early dolomitization and the preservation of early dolomite textures with a higher porosity. The relative scarcity of mud in the crinkly laminite facies further contributes to its good reservoir properties. In contrast, higher flux of fine-grained carbonate in overlying massive and laminated dolostones reduced permeability in these facies, which act as a low-permeability barrier for reservoir unit A. The thick A5 evaporite unit forms the ultimate seal for the A4C.

Distribution of organic material and fine-grained carbonate was linked to the sequence stratigraphy and environmental conditions of the A4C. The position of crinkly laminites in a late TST implies a broad lateral distribution over much of the Birba area (Figs. 12 and 13). This was also a time of reduced flux of clastic carbonate, which allowed significant accumulation of organic material. Environmental conditions conducive to the formation and preservation of organic-rich carbonate laminites, i.e., minimal or absent biological and physical disturbance of sediments, and a stratified water body, are recurrent themes in hydrocarbon-producing basins. Such conditions have been described from evaporitic (e.g., Davies and Ludlam, 1973; Jin and Bergman, 1999; Pope et al., 2000) and non-evaporitic settings (e.g., Knoll et al., 1995). Furthermore, laminated carbonates in sub-wave-base settings are common in many Precambrian platforms (Grotzinger and James, 2000, and references therein), owing to the absence of bioturbating organisms, and irrespective of the development of stratified water masses. In this regard, the earliest Cambrian A4C and younger laminated carbonates, although they may have formed under particular environmental conditions (e.g., stratified water column), are reminiscent of conditions that were ubiquitous in the Precambrian.

6. Conclusions

The A4 unit represents a single depositional sequence in which accommodation was driven by mostly tectonic subsidence. Evaporites were deposited in LST and TST positions, and carbonates formed in TST and HST positions. Within the A4C, the TST was characterized by finely laminated carbonates and sulfates forming an extensive and uniform sheet of outer ramp facies across the Birba area. During the initial stages of transgression, lamination was created by alternating deposition of sulfate cumulates, organic-rich carbonates and detrital fine-grained carbonate. Later in the TST, organic-rich carbonates and detrital carbonate alternate, forming a prolific reservoir facies at the time of maximum flooding and minimal deposition of detrital fine-grained carbonate.

During the highstand, sedimentation of increasingly large volumes of fine-grained carbonate dominated the depositional environment and diluted organic accumulation once sediment export from proximal parts of the platform was established. The late HST was characterized by laminated and cross-laminated fine-grained carbonates, dolarenites and stromatolites that formed in response to storm and wave action above the fair-weather wave-base. Their alternation led to a more complex lithofacies pattern. Late highstand deposition was accompanied by progressive restriction of the basin and a gradual change to renewed evaporite deposition. The overlying LST evaporite unit was deposited *on top* of the former carbonate platform. Strong tectonic subsidence and transient flooding are likely mechanisms to generate this relationship between carbonates and evaporites.

Platform architecture and facies correspond to a low-energy carbonate ramp influenced by storms

and waves. During the highstand, fine-grained carbonate was produced in abundance over most of the middle and inner ramp. Storm- and wave-generated currents distributed it across many of these geomorphic positions. In contrast, transgressive deposits formed under conditions of low sediment flux when sediments were trapped in aerially restricted inner ramp positions close to the shelf edge. The scarcity of fine-grained carbonate in the crinkly laminite reservoir facies contributed directly to its present-day reservoir quality. These facies form a transgressive sheet and drilling has proven its wide lateral distribution on the Birba platform. Organic material accumulated under conditions of reduced biogenic and physical disturbance of sediment and/or a stratified water column. The presence of organic material influenced early dolomitization and led to a porous dolostone, whereas overlying fine-grained massive dolostones form a low-permeability barrier. In contrast, diagenetic evaporite formation strongly degraded reservoir quality in the porous shallow-water facies near the top of the A4C.

Acknowledgements

Logistic and financial support was provided by Petroleum Development Oman, LLC. This study was supported by grants from the Swiss National Science Foundation to A. Matter (grant 20-56791.99) and by NASA grant NAG5-9445 to J. P. Grotzinger. The Ministry of Oil and Gas of the Sultanate of Oman is acknowledged for permission to publish the results of this research. Editorial comments by C. Cowan, B. W. Sellwood, T. Simo and by two anonymous reviewers improved an earlier version of the manuscript.

References

Adams, E.W., Schröder, S., Grotzinger, J.P., McCormick, D.S., 2004. Digital reconstruction and stratigraphic evolution of a microbial-dominated isolated carbonate platform (terminal Proterozoic, Nama Group, Namibia). Journal of Sedimentary Research 74, 479–497.

Aigner, T., 1985. Storm depositional systems. Lecture Notes in Earth Sciences, vol. 1. Springer, Berlin.

Aitken, J.D., 1967. Classification and environmental significance of cryptalgal limestones and dolomites, with illustrations from the Cambrian and Ordovician of SW Alberta. Journal of Sedimentary Petrology 37, 1163–1178.

Amthor, J.E., Grotzinger, J.P., Schröder, S., Bowring, S.A., Ramezani, J., Martin, M.W., Matter, A., 2003. Extinction of *Cloudina* and *Namacalathus* at the Precambrian–Cambrian boundary in Oman. Geology 31, 431–434.

Amthor, J.E., Ramseyer, K., Faulkner, T., Lucas, P., 2005. Stratigraphy and sedimentology of a chert reservoir at the Precambrian–Cambrian Boundary: the Al Shomou Silicilyte, South Oman Salt Basin. GeoArabia 10, 89–122.

Anderson, R.Y., Dean, W.E., Kirkland, D.W., Snider, H.I., 1972. Permian Castile varved evaporite sequence, West Texas and New Mexico. Geological Society of America Bulletin 83, 59–86.

Aurell, M., Bádenas, B., Bosence, D.W.J., Waltham, D.A., 1998. Carbonate production and offshore transport on a Late Jurassic carbonate ramp (Kimmeridgian, Iberian Basin, NE Spain): evidence from outcrops and computer modeling. In: Wright, V.P., Burchette, T.P. (Eds.), Carbonate Ramps, Geological Society of London, Special Publication, vol. 149, pp. 137–161.

Baker, P.A., Kastner, M., 1981. Constraints on the formation of sedimentary dolomite. Science 213, 214–216.

Black, M., 1933. The algal sediments of Andros Island, Bahamas. Philosophical Transactions of the Royal Society of London. Series B 222, 165–192.

Burchette, T.P., Wright, V.P., 1992. Carbonate ramp depositional systems. Sedimentary Geology 79, 3–57.

Burns, S.J., Matter, A., 1993. Carbon isotopic record of the latest Proterozoic from Oman. Eclogae Geologicae Helvetiae 86, 595–607.

Calvet, F., Tucker, M.E., 1988. Outer ramp cycles in the Upper Muschelkalk of the Catalan Basin, northeast Spain. Sedimentary Geology 57, 185–198.

Chafetz, H.S., Buczynski, C., 1992. Bacterially induced lithification of microbial mats. Palaios 7, 277–293.

Chafetz, H.S., Folk, R.L., 1984. Travertines: depositional morphology and the bacterially constructed constituents. Journal of Sedimentary Petrology 54, 289–316.

Cook, H.E., Mullins, H.T., 1983. Basin margin environment. In: Scholle, P.A., Bebout, D.G., Moore, C.H. (Eds.), Carbonate Depositional Environments, American Association of Petroleum Geologists Memoir, vol. 33, pp. 539–617.

Cowan, C.A., James, N.P., 1992. Diastasis cracks: mechanically generated synaeresis-like cracks in Upper Cambrian shallow water oolite and ribbon carbonates. Sedimentology 39, 1101–1118.

Davies, G.R., Ludlam, S.D., 1973. Origin of laminated and graded sediments, Middle Devonian of Western Canada. Geological Society of America Bulletin 84, 3527–3546.

Decima, A., McKenzie, J.A., Schreiber, B.C., 1988. The origin of "evaporative" limestones: an example from the Messinian of Sicily (Italy). Journal of Sedimentary Petrology 58, 256–272.

Demicco, R.V., Hardie, L.A., 1995. Sedimentary structures and early diagenetic features of shallow marine carbonate deposits. SEPM Atlas Series, vol. 1. SEPM, Tulsa.

DiBenedetto, S., Grotzinger, J.P., in press. Geomorphic evolution of a storm-dominated carbonate ramp (c. 549 Ma), Nama Group, Namibia. Geological Magazine.

Elrick, M., Read, J.F., 1991. Cyclic ramp-to-basin carbonate deposits, Lower Mississippian, Wyoming and Montana: a combined field and computer modeling study. Journal of Sedimentary Petrology 61, 1194–1224.

Fairchild, I.J., Herrington, P.M., 1989. A tempestite–stromatolite–evaporite facies association (Late Vendian, East Greenland): a shoreface–lagoon model. Precambrian Research 43, 101–127.

Gallardo, V.A., 1977. Large benthic microbial communities in sulphide biota under Peru–Chile subsurface countercurrent. Nature 268, 331–332.

Gorin, G.E., Racz, L.G., Walter, M.R., 1982. Late Precambrian–Cambrian Sediments of Huqf Group, Sultanate of Oman. American Association of Petroleum Geologists Bulletin 66, 2609–2627.

Grotzinger, J.P., 1989. Facies and evolution of Precambrian depositional systems: emergence of the modern platform archetype. In: Crevello, P.D., Wilson, J.L., Sarg, J.F., Read, J.F. (Eds.), Controls on Carbonate Platform and Basin Development, SEPM Special Publication, vol. 44, pp. 79–106.

Grotzinger, J.P., Amthor, J.E., 2002. Facies and reservoir architecture of isolated microbial carbonate platforms, terminal Proterozoic–Early Cambrian Ara Group, South Oman Salt Basin. AAPG Annual Conference. American Association of Petroleum Geologists, Houston.

Grotzinger, J.P., James, N.P., 2000. Precambrian carbonates: evolution of understanding. In: Grotzinger, J.P., James, N.P. (Eds.), Carbonate Sedimentation and Diagenesis in the Evolving Precambrian World, SEPM Special Publication, vol. 67, pp. 3–20.

Grotzinger, J.P., Kasting, J.F., 1993. New constraints on Precambrian ocean composition. Journal of Geology 101, 235–243.

Grotzinger, J.P., Knoll, A.H., 1999. Stromatolites in Precambrian carbonates: evolutionary mileposts or environmental dipsticks? Annual Review of Earth and Planetary Sciences 27, 313–358.

Grotzinger, J.P., Adams, E.W., Schröder, S., in press. Microbial-metazoan reefs of the terminal Proterozoic Nama Group (ca. 550–543 Ma), Namibia. Geological Magazine.

Hardie, L.A., 1977. Algal structures in cemented crusts and their environmental significance. In: Hardie, L.A. (Ed.), Sedimentation on the Modern Carbonate Tidal Flats of Northwest Andros Islands; Bahamas, The Johns Hopkins University Studies in Geology, vol. 22. Johns Hopkins University Press, Baltimore, pp. 159–177.

Hardie, L.A., Ginsburg, R.N., 1977. Layering: the origin and environmental significance of lamination and thin bedding. In: Hardie, L.A. (Ed.), Sedimentation on the Modern Carbonate Tidal Flats of Northwest Andros Islands; Bahamas, The Johns Hopkins University Studies in Geology, vol. 22. Johns Hopkins University Press, Baltimore, pp. 50–123.

Hofmann, H.J., Mountjoy, E.W., 2001. *Namacalathus–Cloudina* assemblage in Neoproterozoic Miette Group (Byng Formation), British Columbia: Canada's oldest shelly fossils. Geology 29, 1091–1094.

Jin, J., Bergman, K.M., 1999. Sequence stratigraphy of the Middle Devonian Winnipegosis Carbonate–Prairie Evaporite transition, Southern Elk Point Basin. Carbonates and Evaporites 14, 64–83.

Jones, B., 2005. Dolomite crystal architecture: genetic implications for the origin of the Tertiary dolostones of the Cayman Islands. Journal of Sedimentary Research 75, 177–189.

Kendall, A.C., 1992. Evaporites. In: Walker, R.G., James, N.P. (Eds.), Facies Models—Response to Sea Level Change. Geological Association of Canada, St. John's, pp. 375–409.

Knoll, A.H., Grotzinger, J.P., Kaufman, A.J., Kolosov, P., 1995. Integrated approaches to terminal Proterozoic stratigraphy: an example from the Olenek Uplift, northeastern Siberia. Precambrian Research 73, 251–270.

Land, L.S., 1982. Dolomitization. American Association of Petroleum Geologists Education Course Notes Series 24, 1–20.

Loosveld, R., Bell, A., Terken, J., 1996. The tectonic evolution of interior Oman. GeoArabia 1, 28–51.

Lowenstein, T.K., Hardie, L.A., 1985. Criteria for the recognition of salt-pan evaporites. Sedimentology 32, 627–644.

Lucia, F.J., 1995. Rock–fabric/petrophysical classification of carbonate pore space for reservoir characterization. American Association of Petroleum Geologists Bulletin 79, 1275–1300.

Mattes, B.W., Conway Morris, S., 1990. Carbonate/evaporite deposition in the Late Precambrian–Early Cambrian Ara Formation of Southern Oman. In: Robertson, A.H.F., Searle, M.P., Ries, A.C. (Eds.), The Geology and Tectonics of the Oman Region, Geological Society of London, Special Publication, vol. 49, pp. 617–636.

Murray, R.C., Lucia, F.J., 1967. Cause and control of dolomite distribution by rock selectivity. Geological Society of America Bulletin 78, 21–36.

Pelechaty, S.M., Grotzinger, J.P., Kashirtsev, V.A., Zhernovsky, V.P., 1996. Chemostratigraphic and sequence stratigraphic constraints on Vendian–Cambrian basin dynamics, Northeast Siberian Craton. Journal of Geology 104, 543–563.

Pope, M., Grotzinger, J.P., 2000. Controls on fabric development and morphology of tufas and stromatolites, uppermost Pethei Group (1.8 Ga), Great Slave Lake, northwest Canada. In: Grotzinger, J.P., James, N.P. (Eds.), Carbonate Sedimentation and Diagenesis in the Evolving Precambrian World, SEPM Special Publication, vol. 67, pp. 103–122.

Pope, M., Grotzinger, J.P., Schreiber, B.C., 2000. Evaporitic subtidal stromatolites produced by in situ precipitation: textures, facies associations, and temporal significance. Journal of Sedimentary Research 70, 1139–1151.

Read, J.F., 1985. Carbonate platform facies models. American Association of Petroleum Geologists Bulletin 69, 1–21.

Reid, R.P., Macintyre, I.G., 2000. Microboring versus recrystallization: further insight into the micritization process. Journal of Sedimentary Research 70, 24–28.

Robbins, L.L., Blackwelder, P.L., 1992. Biochemical and ultrastructural evidence for the origin of whitings: a biologically induced calcium carbonate precipitation mechanism. Geology 20, 464–468.

Sarg, J.F., 2001. The sequence stratigraphy, sedimentology, and economic importance of evaporite–carbonate transitions: a review. Sedimentary Geology 140, 9–42.

Schreiber, B.C, 1978. Environments of subaqueous gypsum deposition. In: Dean, W.E., Schreiber, B.C. (Eds.), Marine Evaporites, SEPM Short Course, vol. 4, pp. 43–73.

Schreiber, B.C., Kinsman, D.J.J., 1975. New observations on the Pleistocene evaporites of Montallegro, Sicily and a modern analog. Journal of Sedimentary Petrology 45, 469–479.

Schröder, S., 2000. Reservoir quality prediction in Ara Group carbonates of the South Carbonate Platform, South Oman Salt Basin. PhD thesis, University of Bern.

Schröder, S., Schreiber, B.C., Amthor, J.E., Matter, A., 2003. A depositional model for the terminal Neoproterozoic–Early Cambrian Ara Group evaporites in south Oman. Sedimentology 50, 879–898.

Schulz, H.N., Brinkhoff, T., Ferdelman, T.G., Hernández Mariné, M., Teske, A., Jørgensen, B.B., 1999. Dense populations of a giant sulfur bacterium in Namibian shelf sediments. Science 284, 493–495.

Shinn, E.A., Steinen, R.P., Lidz, B.H., Swart, P.K., 1989. Whitings, a sedimentological dilemma. Journal of Sedimentary Petrology 59, 147–161.

Sibley, D.F., Gregg, J.M., 1987. Classification of dolomite rock texture. Journal of Sedimentary Petrology 57, 967–975.

Slaughter, M., Hill, R.J., 1991. The influence of organic matter in organogenic dolomitization. Journal of Sedimentary Petrology 61, 296–303.

Smoot, J.P., Castens-Seidell, B., 1994. Sedimentary features produced by efflorescent salt crusts, Saline Valley and Death Valley, California. In: Renaut, R.W., Last, W.M. (Eds.), Sedimentology and Geochemistry of Modern and Ancient Saline Lakes, SEPM Special Publication, vol. 50, pp. 73–90.

Southard, J.B., Lambie, J.M., Federico, D.C., Pile, H.T., Weidman, C.R., 1990. Experiments on bed configurations in fine sands under bidirectional purely oscillatory flow, and the origin of hummocky cross-stratification. Journal of Sedimentary Petrology 60, 1–17.

Suhayda, J.N., 1977. Surface waves and bottom sediment response. Marine Geotechnology 2, 135–146.

Tucker, M.E., 1991. Sequence stratigraphy of carbonate–evaporite basins: models and application to the Upper Permian (Zechstein) of northeast England and adjoining North Sea. Journal of the Geological Society 148, 1019–1036.

Tucker, M.E., 1992. The Precambrian–Cambrian boundary: seawater chemistry, ocean circulation and nutrient supply in metazoan evolution, extinction and biomineralization. Journal of the Geological Society 149, 655–668.

Tucker, M.E., Calvet, F., Hunt, D., 1993. Sequence stratigraphy of carbonate ramps: systems tracts, models and application to the Muschelkalk carbonate platforms of eastern Spain. In: Posamentier, H.W., Summerhayes, C.P., Haq, B.U., Allen, G.P. (Eds.), Sequence Stratigraphy and Facies Associations, IAS Special Publication, vol. 18, pp. 397–415.

Turner, E.C., James, N.P., Narbonne, G.M., 1997. Growth dynamics of Neoproterozoic calcimicrobial reefs, Mackenzie Mountains, Northwest Canada. Journal of Sedimentary Research 67, 437–450.

Watters, W.A., Grotzinger, J.P., 2001. Digital reconstruction of calcified early metazoans, terminal Proterozoic Nama Group, Namibia. Paleobiology 27, 159–171.

Wilson, J.L., 1975. Carbonate Facies in Geologic History. Springer-Verlag, Berlin.

Wood, R.A., Grotzinger, J.P., Dickson, J.A.D., 2002. Proterozoic modular biomineralized metazoan from the Nama Group, Namibia. Science 296, 2383–2386.

Wright, V.P., Faulkner, T.J., 1990. Sediment dynamics of Early Carboniferous ramps: a proposal. Geological Journal 25, 139–144.